Invited Articles

Advances in understanding the role of salt and surfactants on aerosol and drop emission by collective bubble bursting

Tristan Aurégan,* Megan Mazzatenta,* and Samuel M. Koblensky
Department of Mechanical and Aerospace Engineering, Princeton University, Princeton, New Jersey 08544, USA

Luc Deike†
Department of Mechanical and Aerospace Engineering, Princeton University, Princeton, New Jersey 08544, USA
and High Meadows Environmental Institute, Princeton University, Princeton, New Jersey 08544, USA

(Received 12 June 2026; accepted 1 October 2026; published 16 November 2026)

Drop production from bursting bubbles is fundamental to understand sea salt and organic aerosol production or the transport of pathogens and aroma. However, the virtually unavoidable presence of contaminants in practical situations means that processes at the scale of the films, bubbles, and rafts are influenced by surface-active agents and salts. In this perspective, we review recent experimental and numerical advances in the understanding of drop production in the presence of contamination. We start from classical relationships that quantitatively describe drop production in the absence of contamination and then review how processes at different scales are modified. At the individual bubble scale, jet drop formation is altered in a nonuniform manner, and film drop formation is subjected to modification of bubble drainage and lifetime. At the collective level, we separate effects of polydisperse, oceanlike bubble size distributions, and monodisperse, champagnelike bubble size distributions. For oceanlike polydisperse bubble size distributions, we discuss how surfactants increase film drop production and suppress jet drops, while large increases in salt concentration result in similar sized but more numerous aerosols. For sparkling winelike monodisperse bubble rafts, we review collective effects due to neighboring bubbles acting on the cavity collapse and linked to a strong reduction of jet drop size.

DOI: 10.1103/tv7k-pz1n

I. INTRODUCTION

A. Motivation

Bubbles bursting at the surface of the ocean following air entrained by breaking waves or at the surface of a champagne glass have attracted the attention of the fluid dynamics community for decades [1,2]. Describing the fate of a bubble which rises to the surface, settles for some finite time, bursts, and ejects drops requires the understanding of interfacial fluid mechanics processes

*These authors contributed equally to this work.
†Contact author: ldeike@princeton.edu

Published by the American Physical Society under the terms of the Creative Commons Attribution 4.0 International license. Further distribution of this work must maintain attribution to the author(s) and the published article's title, journal citation, and DOI.

over a wide range of scales and regimes. The motivation has come from fundamental questions such as describing similarity solutions [3–5], drainage of thin films [6], rupture [7], identification of instabilities responsible for bursting and drop size selection [1], as well as practical implications. The ejected drops and aerosols transport aroma, playing a role in champagne tasting [8,9], and can transport pathogens with implications for disease transmission [10,11]. Bubble bursting at the ocean surface controls the emission of marine aerosols, made of sea salt and organics [12,13]. The number, size, and composition of marine aerosols then determine their ability to serve as cloud condensation nuclei or ice nucleating particles, as well as to directly affect the radiative balance. Previous reviews have extensively documented the various modes of emission of drops in the ocean in the absence of surfactants [12,14–16].

Our fundamental understanding of bubble bursting is primarily based on canonical configurations where individual bubble bursting was studied and modes of drop production were identified, namely jet and film drop production, where each mode operates for specific ranges of the controlling physical parameters. Jet drops are formed by bubbles of sizes ranging from a few tens of microns to several millimeters (capillary length), and these drops are mostly supermicron in size [9,13,17,18]. In contrast, film drops are produced by bubbles from about 100 microns to a few millimeters and can be as small as a few hundred of nanometers [7,13,19,20].

Considering a bubble of radius R_b bursting at the interface between a liquid and air, the problem can be defined in terms of a set of nondimensional numbers: the density ratio, the viscosity ratio, and the ratio of the bubble size over two characteristic lengths, the capillary length (leading to the Bond number), and the viscocapillary length (leading to the Laplace number or Ohnesorge number). The goal is then to predict the mean size of the ejected drops $r_d(R_b)$, their number $n_d(R_b)$, and their size distribution $p(r_d, R_b)$ as a function of the physical properties of the fluid (typically surface tension, viscosity, and density). Building on extensive laboratory experiments and high-fidelity numerical simulations, scaling theories have been proposed separately for jet and film drop production [6,15,20–22]. Additional, indirect parameters such as the lifetime of the surface bubbles and the thickness of the film at burst have also been identified as key parameters determining the number and size of film drops.

However, the practical configurations mentioned above (such as bubble bursting at the ocean surface or in a glass of champagne), all include contamination of the fluid or interface by surface-active molecules, or surfactants, at the surface. These surfactants can drive Marangoni stresses, lead to non-Newtonian rheology in the bulk [23,24], or can form a layer of oil at the surface [25,26]. The resulting parameter space becomes enormous and the connection to the original motivating problem is nontrivial. We focus in this perspective on surfactant effects on bubble bursting.

The presence of surfactant is known to modulate multiple aspects of the bubbles' dynamics: The rise velocity is reduced by changing the mobility of the interface and associated drag [27,28], the lifetime at the surface is increased by altering film drainage [10], coalescence with neighboring bubbles is suppressed leading to the emergence of rafts [29], and finally the dynamics of bursting itself can be altered [30]. All of these effects will directly or indirectly modify the final aerosol emissions in presence of surfactant.

Identifying the appropriate characteristics of surfactant that control aerosol emissions is therefore a remarkable challenge, as surfactants' effects on these various subprocesses cannot be described by a single surfactant parameter. Connecting experimental results to theoretical background is also complicated, as experimental results are often reported in terms of surfactant concentration, while theoretical and numerical frameworks require knowledge of surfactant in terms of constitutive laws. Practical configurations will involve complex mixtures of surfactants and salts (which are central to the ocean context and also interact with ionic surfactants), compared to idealized solutions studied in the laboratory.

The other connected question is the role of collective effects on bubble bursting and aerosol emission. In practice, bubbles are not alone but rise in groups and then organize in rafts at the surface. Water contamination modulates possible collective effects, as it increases bubble lifetime and prevents coalescence, leading to densely packed rafts (where ejection can be enhanced) and

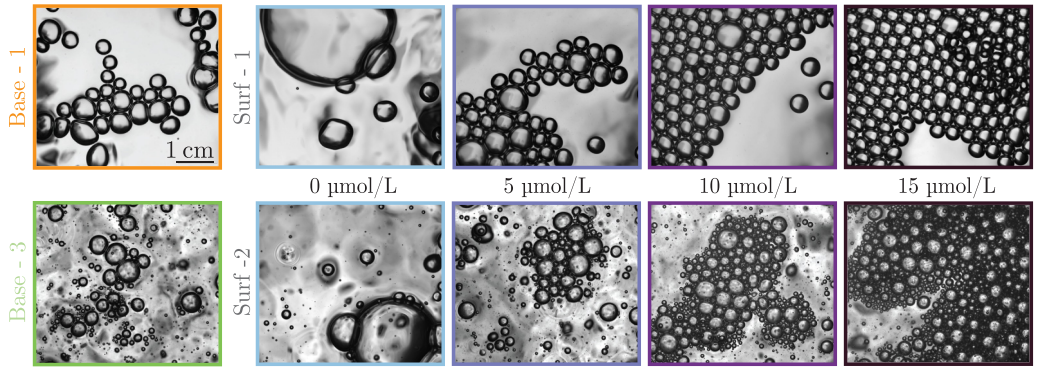


FIG. 1. Examples of surface bubbles views. Left column shows examples of narrow (Base-1) and broad-banded (Base-3) distributions. Other panels show the effect of increasing surfactant concentration [here sodium dodecyl sulfate (SDS) is used] in narrow-banded (Surf-1) and broad-banded cases (Surf-2). All images have the same scale.

even multilayer foams (where ejection tends to be suppressed) [31]. We will discuss how much collective effects should be accounted for in various practical configurations, depending on the size distribution of bubbles, either polydisperse (like at the ocean surface) or more monodisperse (like in the champagne glass).

The aim of the present perspective is to review recent results on the role of surfactant and salt in bubble bursting and sea spray emissions in terms of both individual effects and collective effects. We organize the results around a set of canonical configurations: salty, oceanlike broad-banded bubble size distributions (Fig. 1, bottom row) and champagnelike, quasimonodisperse rafts (Fig. 1, top row). We discuss how much understanding from individual bursting can be applied to collective bursting, as well as additional effects of surfactant and salt.

B. From one bubble to an ensemble of bubbles

For a specific drop production process, the total drop size distribution $N_d(r_d)$ produced by an ensemble of bursting bubbles is obtained by integrating individual bursting scalings over the size distribution of bursting bubbles at the surface $N_b(R_b)$ in the size range given by $R_{b,\min}$ and $R_{b,\max}$, given by the following equation [6,14,15]:

$$N_d(r_d) = \int_{R_{b,\min}}^{R_{b,\max}} \frac{N_b(R_b) n_d(R_b)}{\langle r_d \rangle (R_b)} p\left(\frac{r_d}{\langle r_d \rangle}, R_b\right) \mathrm{d}R_b, \tag{1}$$

where n_d, $\langle r_d \rangle$, and $p(r_d/\langle r_d \rangle, R_b)$ are the number, mean size, and drop size distribution associated with one mode of drop production, respectively. In addition, $R_{b,\min}$ and $R_{b,\max}$ are the size limits where one mode of drop production happens.

In order to predict the overall drop size distribution we therefore need to know the expected scalings of the drop parameters (number, mean size, and distribution) with the bubble size. In the following, we review classical results for each mode of production (detailed discussions on the choice of each of the parameters can be found in Deike *et al.* [15] and Mazzatenta *et al.* [32]).

The scope of the review will be to assess how this framework needs to be modified for different types of contamination, for different shapes of the bubble size distribution leading to collective effects or not, and to determine which variables in Eq. (1) are affected by salt or surfactant (for each mode of production).

C. Jet drops

Jet drops are produced through the destabilization of a jet formed during the collapse of the underwater cavity remaining after the cap of a bubble has retracted [5,9,17,33–40]. For a bubble of radius R_b with a liquid of density ρ, viscosity μ, and surface tension γ, the governing nondimensional numbers of the dynamics are the Bond ($\mathrm{Bo} = R_b^2/\ell_c^2$) and Laplace ($\mathrm{La} = R_b/\ell_\mu$) numbers, with $\ell_c = \sqrt{\gamma/\rho g}$ the capillary length and $\ell_\mu = \mu^2/\gamma\rho$ the viscocapillary length (g is the gravitational constant and ρ, γ, and μ are the density, surface tension, and viscosity of the liquid, respectively). The Bond number compares the magnitude of gravitational and interfacial forces, while the Laplace number compares interfacial and viscous forces. Jet drops in water are typically formed for bubbles with radius between 10 and 20 μm (La above 600) and the capillary length [38,41]. There are several formulas describing the size of the emitted drops [21,22,38,42], obtained from theoretical scaling laws with final adjustment of a parameter on the same experimental and computational data. We use the formulation initially developed by Gañán-Calvo [21], $\langle r_d\rangle = \chi_1\ell_\mu(\sqrt{\mathrm{La}}(\sqrt{\mathrm{La}/\mathrm{La}_\star}-1))^{5/4}$, with χ_1 a numerical prefactor and $\mathrm{La}_\star = 500$ the La number below which no drop is ejected. The number of produced drops follows $n_d = \chi_2(R_b/\ell_\mu)^{-1/3}$, a scaling initially proposed by Berny *et al.* [39], with a prefactor adapted based on recent experimental data from Mazzatenta *et al.* [32] and Wang *et al.* [43], Chu *et al.* [44], and Wang *et al.* [45]. A table of all prefactor values for the classical case without surfactants is provided in the Appendix (Table II).

D. Film drops

Film drops refer to drops originating from the film separating the bubble at the surface before it bursts and have long been recognized as dominating the submicron sea salt aerosol production, coming from bubbles as small as tens of microns and up to several millimeters [12,13].

Multiple modes of film drop production have been discussed, in particular film centrifuge in large bubbles where the nearly hemispherical bubble cap retracts and destabilizes into drops and film flap where the instability occurs in smaller bubbles in a manner similar to a flat film. Both of these mechanisms are thought to strongly depend on the thickness of the bubble cap at the instant the bubble bursts (h_b).

Film centrifuge drop production has been described in detail [6,7,46,47] from bubbles with radii $R_b > 0.2\ell_c$. The number and mean size associated with this mode of production was originally described by Lhuissier and Villermaux [6]: $\langle r_d\rangle = \chi_3 R_b^{3/8}h_b^{5/8}$ and $n_d = \chi_4(R_b/\ell_c)^2(R_b/h_b)^{7/8}$, with χ_3 and χ_4 fitted constants. Fluctuations of temperature and contamination in the cap are thought to lead to Marangoni stresses that trigger the rupture of the cap, resulting in the semiempirical fitting $h_b = \chi_5 R_b^2/\ell_c$, compatible with experiments for large bubbles in Shaw and Deike [47], with a prefactor χ_5 that varies with temperature.

The film flapping mechanism has been proposed by Jiang *et al.* [20] in an effort to explain the observation of submicron dry particles in bubbling tank experiments that cannot be described by the previous mechanisms. Following the empirical relationships developed in Deike *et al.* [15] using data from Jiang *et al.* [20] and Lewis and Schwartz [13], this mechanism is hypothesized to occur for bubble with radii between 70 and 1000 μm, producing $n_d \approx 40$ drops of mean size $\langle r_d\rangle \sim h_b\sqrt{\rho_a/\rho}$, with ρ_a the density of the surrounding air. The thickness at burst needs to be estimated again and has not been measured directly for bubbles in that size range. Using data from Jiang *et al.* [20], an empirical relationship, $\langle r_d\rangle = \chi_6\ell_c(R_b/\ell_c)^{1/3}$, has been proposed in Deike *et al.* [15] (without physical justification). Note that this latter relationship fitted on data for very small bubbles is, however, not consistent with the scaling for bursting thickness mentioned above. A related separate pathway is discussed in Jiang *et al.* [48]: Underwater collisions between bubbles lead to the formation of a thin liquid film that ruptures at coalescence, embedding droplets into rising bubbles, which would then be released as film drops during bursting.

E. How to describe the effect of surfactant on aerosol emissions?

As mentioned earlier, at the ocean surface or in industrial applications, interfaces are often contaminated with surfactants. The surfactant surface concentration Γ affects the surface tension of the interface via some equation of state $\gamma = \gamma(\Gamma)$, often referred to as the surface tension isotherm [49]. Surfactants are transported at the surface and surface tension gradients resulting from surface concentration inhomogeneities then give rise to Marangoni stresses [28,50,51]. These stresses are often quantified through the Marangoni number [49] comparing the intensity of surfactant gradients to a restoring or limiting force (e.g., shear or diffusion).

Quantitative comparisons between experiments and numerical simulations have remained limited [52] as experiments report the surfactant bulk concentration without having access to spatial and temporal variations in surface concentration and the surfactant equation of state is not always available. Separately, two-phase Navier-Stokes simulations with surfactant transport and Marangoni stresses enable detailed access to the surfactant dynamics but require assumptions on the effect of surfactant on the interfacial dynamics.

A link between experiments and theories or computations can then be made in the case of insoluble surfactant through the use of a measured equation of state $\gamma = \gamma(\Gamma)$ [49], effectively defining a Marangoni number using experimentally measured relative surface tension variations with surface concentration. Such an approach was used to interpret surfactant effects on surface waves including damping of parasitic capillary waves and breaking [51,53], jet drop production by bubble bursting with quantitative comparison between experiments and computations [54], as well as qualitative features of the rise dynamics of underwater bubbles in quiescent flow [28].

While Marangoni stresses in the context of insoluble surfactants provide an accurate framework to describe surfactant effects on jet drops or breaking waves, processes that occur on a slower timescale or that involve fast-adsorbing surfactants require a more complex description. In that case, solubility may play a key role in the dynamics, and fluxes between the bulk and the interfaces need to be considered, further increasing the size of the parameter space. In practice, surfactants have distinct chemical properties, which govern their physicochemical behavior [49,55].

For example, the solubility (adsorption equilibrium constants) of biological surfactants, including polysaccharides, lipids, proteins, and humics, in the ocean can vary by several orders of magnitude [56]. This variation leads to differences in the relative abundance of the compounds between ocean surface water and sea spray aerosols. Recent experimental work suggest the adsorption-desorption characteristic time (or length) plays a role in modulating bubble break-up in turbulence [57] and thinning and rupture of Savart sheets [58].

In addition, there are classes of problems where the framework involving the Marangoni number or even the solubility does not seem suited to describe the observed physics. In particular problems involving thin films (through their drainage or through spontaneous rupture) generally do not exhibit simple dependence with the parameters mentioned above and instead seem very sensitive to minute experimental details [46,59]. For instance the use of tap water (or the introduction of salts) can drastically alter bubble lifetime compared with using deionized water at the same surfactant concentration, without measurably changing any of the physical properties of the solution. The presence of impurities may therefore strongly influence these fragile objects.

F. Scope and outline

The present perspective focuses on experimental work and is structured as follows. In Sec. II, we present the various types of experimental setups used to characterize drop and aerosol emissions by bubble bursting. In Sec. III, we present the canonical oceanlike polydisperse configuration where the drop emissions can be explained by Eq. (1) combined with knowledge of the bubble bursting size distribution and the individual bursting scaling laws. In Sec. IV, we present how surfactants and salts can modify individual bubble bursting and subsequent drop production. In Sec. V, we return to the canonical polydisperse configurations and discuss how salts and surfactant can modify the results from the original canonical case and their coherence with the individual bursting results. In

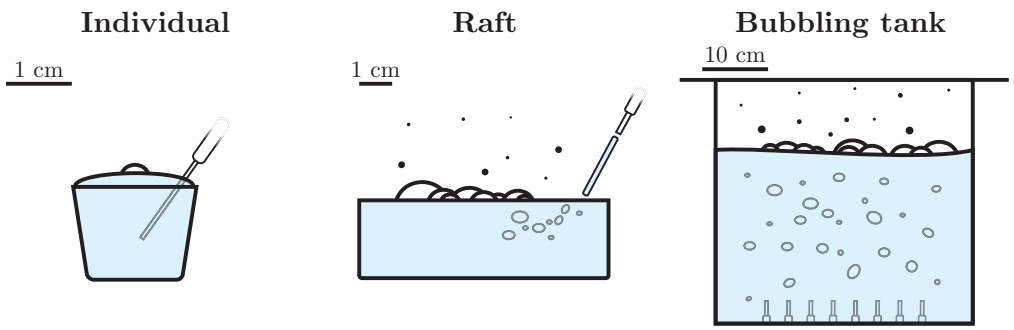


FIG. 2. Schematic representation of the three types of setup used in the studies described in this perspective: Individual where a single bubble is studied, raft where small groups of up to a few hundred bubbles are formed in bursts, and the bubbling tank where bubbles are continuously injected into a large tank. The measurements possible at each scale are also listed.

Sec. VI, we present the case with densely packed monodisperse rafts, found in sparkling drinks, where collective effects become dominant in describing the drop size distribution.

II. EXPERIMENTAL SETUPS

In this section we briefly describe experimental setups that we have used to investigate bubble bursting and drop production. We also introduce notations and quantities used throughout the review.

The experimental setups used to study drop production presented in this perspective can be classified into three broad categories depending on the scale and therefore on the number of bubbles studied (Fig. 2): studies at the individual bubble scale, at the scale of rafts of at most few hundred bubbles and larger-scale bubbling tank experiments, that continuously generate a large number of bubbles. We quickly describe the advantages of each of these scales and the measurements that they allow obtaining.

Experiments at the individual bubble scale allow for a large degree of control over the experimental conditions (bubble size, contamination, etc.) and detailed analysis of the mechanisms at play (drainage, formation of drops, etc.) through high magnification observations. The bubbles used in this type of study typically have a radius from 1 to 10 mm with very few studies using smaller bubble sizes [17,35] due to important experimental challenges. Measurements can access the size r_d and number n_d of drops for each bubble size, as well as the thickness at burst h_b and lifetime. In particular, we have used this type of approach to record surface bubble lifetime and cap drainage across various types of contamination [59] and the production of the jet [54] and film drops [47] using high speed imaging.

Experiments at the scale of small rafts incorporate bubble interactions during drainage and bursting. These experiments are typically done by injecting a limited number of bubbles (up to few hundred) either through a plunging jet or with a needle and then observing the raft decay until all bubbles have spontaneously burst. Experiments that record both raft geometry and drop sizes and velocities have allowed us to show that these interactions can drastically influence drop production [60]. In addition, the larger number of bubbles present (and therefore of droplets) allows for a faster recording compared to single bubble experiments that have to be repeated a large number of times. As a consequence they can be used to measure bubble lifetime in a broad range of bubble sizes by observing the decay rate of certain sizes of bubble within a polydisperse raft. Similarly, they can be

used to study the drop size distribution N_d produced from ensembles of bubbles, with a setup easier to handle than bubbling tank experiments, and can keep track of the dynamics of the raft [29].

Finally, the bubbling tank experiments have the highest fidelity to oceanic applications and require the fewest number of assumptions about the problem. Bubbles are continuously generated at the bottom of a large tank and then rise freely up to the surface (there may be a turbulent flow field underwater that changes the bubble size distribution). They can then coalesce or aggregate into rafts at the surface before bursting and producing drops. The statistical stationarity and high bubble throughput of this experiment allows for long recordings of the various size distributions, ensuring the robustness of the data and measurement in the submicron size range inaccessible to other approaches. This experiment allows to vary and measure the distributions of bulk bubbles N_{bulk}, the resulting surface bubbles N_s, and drops or dried particles N_d, while varying the composition of the solution [31,32,61].

For individual and raft-scale experiments, most measurements are obtained using visual observations of the bubbles and drops using cameras. Drop sizes and velocities are obtained using high speed cameras above the surface, while bubble sizes are obtained using regular cameras looking down on the surface. The thickness of bubble caps can be measured either using the retraction velocity of the film during burst [6,47] or through color interferometry [62,63]. In the bubbling tank experiment, the surface N_s and bulk N_{bulk} bubble size distributions are measured using regular cameras. The drop and aerosol size distribution N_d is measured using a combination tools for different size ranges as all drop sizes cannot be measured with a single technique: The presence of the smallest drops is instead inferred from the measurement of their corresponding dry particles (i.e., the salt crystal left behind after evaporation). In the following we denote the drop size distribution as N_d and the aerosol or dry particle size distribution as N_p. The drop size distribution N_d is only measured directly at large sizes while the dry particle size distribution N_p is only measured directly at smaller sizes. These two distributions can, however, be related as we describe in the following. The largest drops are measured optically using either shadowgraphy or digital inline holography [32,64]. The smaller drops ($\lesssim$5 μm) are measured indirectly using dry particles (which therefore requires using salt in the solution): These dry particles are then measured either by an optical particle sizer (OPS) for the larger ones ($\gtrsim$0.5 μm) or a scanning mobility particle sizer (SMPS) for the smaller ones. These measurements give us the dry particle size distribution N_p, which can then be converted into a drop size distribution. Indeed, salt mass conservation between the drop of radius r_d and its dry particle of radius r_p gives

$$\frac{r_p}{r_d} = \left(\frac{\rho_w}{\rho_{\text{salt}}} S\right)^{1/3}, \tag{2}$$

with S the salinity of the solution (or the weight fraction of salt) and where ρ_w and ρ_{salt} are the densities of the solution and of the dry salt particle, respectively. Measurements of submicron aerosols in bubbling tank by use of an OPS or SMPS are broadly used in the atmospheric aerosol literature [43,44,65,66].

The lifetime of the surface bubbles can be measured in all three setup scales: At the individual bubble scale it is simply done by recording how long bubbles reside on the surface from the moment they reach the surface from the bulk to the spontaneous rupture of the cap. In the raft-scale setup, the number of bubbles in a given bin of bubble radius R_b can be track over time as the raft decays. This gives access to a typical timescale for decay in a raft, as a function of bubble size. Finally, in the bubbling tank setup, a flux argument between rising underwater bubbles and bursting surface bubbles (detailed in Sec. III and in Mazzatenta *et al.* [32]) gives access to a size dependent timescale of residence on the surface. While these three measurement techniques all measure surface bubble lifetime, given the quite different methodologies that they use, we will use different notations within this review: τ_i for the individual bubble setup, τ_d for decaying rafts, and τ_s for the bubbling tank setup.

TABLE I. Summary of the experimental conditions tested in the large-scale experimental setup.

Name	Bubble size distribution	Surfactant	Salt
Base-1	Narrow: 2 to 3 mm	None	Sea salt 35 g/l
Base-2	Narrow: 250 μm	None	Sea salt 35 g/l
Base-3	Broad: 2 to 3 mm	None	Sea salt 35 g/l
Surf-1	Narrow: 2 mm	Sodium dodecyl sulfate (SDS): 0 to 15 μmol/l	Sea salt 35 g/l
Surf-2	Broad: 2 mm	SDS: 0 to 15 μmol/l	Sea salt 35 g/l
Surf-3	Narrow: < 1 mm	SDS: 0 to 50 μmol/l	Sea salt 35 g/l
Surf-4	Narrow: 2 mm	SDS: 0 to 1000 μmol/l	None
Salt-1	Broad: 2 mm	Tween 20: 0.4 μmol/l	Sea salt 10^{-2} to 35 g/l
Salt-2	Broad: 2 mm	Tween 20: 0.4 μmol/l	Sodium acetate 10^{-2} to 22 g/l

We have made several experimental campaigns with the large-scale setup, varying the bubble size distribution, the contamination of the solution, and the salt concentration. Some of them are reported in Néel *et al.* [31] and Mazzatenta *et al.* [32,61] while some of them are original data incorporated in the present perspective.

Comparisons between contaminations used in the laboratory using artificial surfactants with oceanic levels of contamination is difficult. While field campaigns measuring the chemical properties of the sea-surface microlayer exist [67,68], linking those to physical properties of laboratory solutions is often ambiguous and not straightforward. Another approach consists in linking field aerosol production to biological activity with measurements linking an increase of aerosol production during periods of intense biological activity [69,70]. The biological activity is sometimes quantified with concentrations of chlorophyll *a*, again difficult to relate to concentrations of laboratory surfactants.

Example views of the surface are shown in Fig. 1 and the list of different configurations are summarized in Table I. Cases labeled with "Base" correspond to single experiments with no surfactant added beyond those present in the sea salt mixture (ASTM D1141-98 Artificial Sea Salt, which is composed of the same proportions of inorganic salts found in natural seawater), cases "Surf" correspond to sweeps of surfactant concentration with a fixed bubble injection method and salt concentration, and cases "Salt" correspond to sweeps of salt concentration with fixed surfactant concentration and bubble injection. Two general classes of surface configurations exist: the broad-banded cases where bubbles of all sizes between a few tens of microns to a few millimeters can be found (see Base-3 and Surf-2 in Fig. 1 for instance); this case is considered representative of what is found in the ocean where entrainment by breaking and subsurface turbulence results in broad-banded bubble distributions. The other cases are narrow-banded around a mean size that is dictated by method used to generate bubbles (an aquarium bubbler or needles) and representative of the case of sparkling drinks where dissolved gas transfer towards rising bubbles generates a uniform size.

For the "Surf" experiments where surfactant concentration is varied, we use the anionic surfactant sodium dodecyl sulfate (SDS), a well-characterized surfactant [71] previously used in the literature to mimic the lipids existing in natural seawater [56,72]. In the Surf-1, Surf-2, and Surf-3 studies, SDS is added to a base solution of artificial seawater (prepared with a salt concentration of 35 g/l similar to typical ocean conditions), while the Surf-4 cases explore the effect of SDS in solutions without no salt. The "Salt" experiments are sweeps of salt concentration use instead a nonionic surfactant: Tween 20 to minimize interactions with the salts used.

III. THE CANONICAL OCEANLIKE CASE

Using the bubbling tank setup, we present a oceanlike case used to capture several key features of ocean bubbles, defined by collective bursting of polydisperse bubbles in an artificial seawater

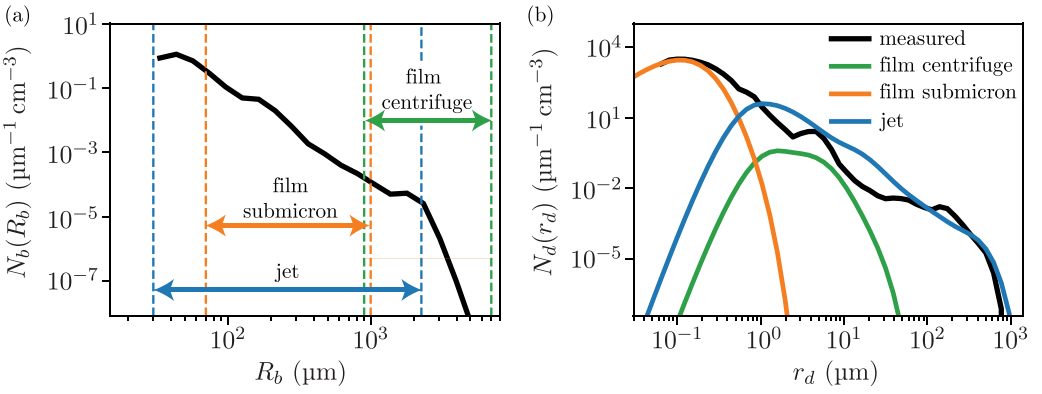


FIG. 3. Measured bubble $N_b(R_b)$ and drop $N_d(r_d)$ size distributions for the oceanlike case of a broad-bubble size distribution in artificial seawater (see case Base-3 in Table I and Fig. 1). Overlaid in color are the drop size distributions predicted with Eq. (1), using the measured bubble size distribution and information from individual bubble bursting mechanisms. Bubble size ranges that can produce drops through each mechanism are labeled in the same color on the measured bubble size distributions.

solution (labeled case Base-3 in Table I and Fig. 1). In this configuration, the broad-banded size distribution of rising bubbles mimics that of bubbles entrained by breaking waves, and surface bubbles cluster in rafts of various sizes before bursting, similarly to their behavior at the air-sea interface. Figure 3 shows the measured bubble size distributions spanning radii 30 to 5000 μm (a) and drop size distributions spanning liquid drop radii 50 nm to 500 μm (b).

Using these detailed measurements, we start by summarizing our understanding of the oceanlike case to analyze the link between measured size distributions of bubbles and drops. In Mazzatenta *et al.* [32], we demonstrated that the spray generation by bursting of these polydisperse bubbles can be well described by Eq. (1), using the measured surface bubble size distribution and scaling laws developed for the bursting of individual bubbles. Variations in drop production due to salts, surfactants, or collective effects in either polydisperse or monodisperse bubble configurations can then be explored.

As discussed in Mazzatenta *et al.* [32], linking the measurements of emitted drops to those of bursting bubbles at the surface or in the bulk requires information on the bubbles' journey of rising and bursting, which can be understood through a flux budget: In the absence of coalescence at the surface and without formation of child bubbles, the flux of bubbles rising through a plane underwater must be equal to the number of bubbles bursting at the surface per unit time. In practice, we use the flux argument to convert the surface bubble size distribution (measured as a number of bubbles per unit area) into a quantity with the same units as the aerosol size distribution (number of aerosols per unit volume), which allows us to directly relate the bursting surface bubbles to the emitted drops. The size distribution of bursting bubbles, $N_b(R_b)$, is then

$$N_b(R_b) = \frac{N_s(R_b)}{\tau_s(R_b)\, w_b(R_b)}, \tag{3}$$

where $N_s(R_b)$ is the measured surface bubble size distribution; $\tau_s(R_b)$ is the lifetime of bubbles at the surface that *a priori* depends on bubble size, surfactant concentration, and salinity [6,59]; and $w_b(R_b)$ is the rise velocity of underwater bubbles that depends on bubble size and can be modified by the turbulence intensity [73–75] or the contamination of the solution [27,76]. For the inorganic artificial seawater solution studied in the this case, we start with an estimate of a constant bubble lifetime of order one second (which will be reassessed once we add surfactant and vary salinity).

When there is no surface coalescence, the distribution normalized in this way is equivalent to the distribution of underwater bubbles N_{bulk}. We can therefore verify the adequacy of our approach

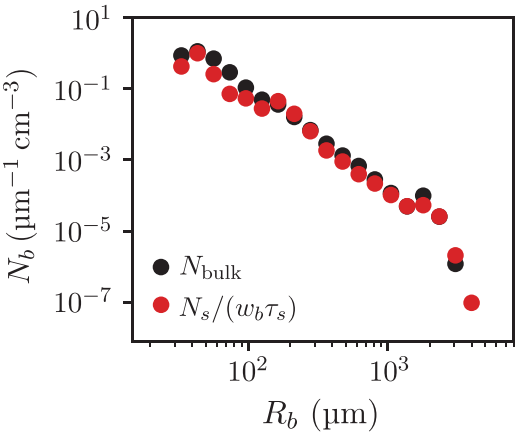


FIG. 4. Comparison between the bulk bubble measurement, $N_{\mathrm{bulk}}(R_b)$, and the converted bursting bubble size distribution, consisting of the surface bubble measurement, $N_s(R_b)$, normalized with the length scale constructed from the size-dependent rise velocity $w_b(R_b)$ and surface bubble lifetime $\tau_s(R_b)$ [following Eq. (3)].

by confirming that these two distributions compare well together, as shown in Fig. 4. The overall agreement in the trends and magnitudes of the distributions indicates that for this artificial seawater solution, coalescence is not a dominant process and constant τ_s is a reasonable approximation. While appropriate for artificial seawater, these assumptions will not always hold, especially when surface bubble behavior is strongly modulated by surfactant; for instance, in dataset Surf-4, the bulk size distribution is (nearly) unchanged for all surfactant concentrations, but the surface bubble size distribution transitions from broad (exponential) due to coalescence to narrow banded as surfactant concentration is increased and coalescence prevented.

We then use the converted surface bubble size distribution to directly link the bursting bubbles to emitted drops and evaluate how well scaling laws developed for individual bubble bursting describe the collective bursting results. Following the approach described in Sec. I B, we use formulations from individual bubble bursting to predict the drop size distribution produced from our measured bubble size distribution, which we then compare to our measured drop size distributions. Figure 3 demonstrates the result of the integration in Eq. (1) for each production mechanism (shown in color) compared to the measured drop size distribution (shown in black) for the canonical ocean case. We find that the experimental drop size distributions can be predicted well from knowledge of the experimental bubble size distributions and scaling laws developed for individual bubble bursting following two modes of drop production—jet drop production for the supermicron drops (summarized in Deike *et al.* [15], with data and scaling laws from several studies [5,9,21,34,37,42]) and submicron film drop production for the smallest drops (in line with experimental data from Jiang *et al.* [20], Chu *et al.* [44], Jiang *et al.* [48])—and can be used as long as the size distribution of bursting surface bubbles is known, while centrifuge drops are not needed to describe the results. These observations hold for a variety of other broad-banded bubble size distributions in artificial seawater [32].

The results summarized in Fig. 3 demonstrate that, for the case of broad-banded bubble size distributions in artificial seawater, drop production by bubble bursting and associated sea spray emission functions can be constructed based on Eq. (1). This construction uses the bursting bubble size distribution and the fitted scaling laws from jet drop and submicron film drop production mechanisms developed for individual bubble bursting. This broad-banded configuration will be referred to as canonical in the following text, where we will now explore the effect of surfactant contamination on collective bubble bursting, which will influence both mechanisms of drop production.

IV. INDIVIDUAL BUBBLE BURSTING

In this section, we review recent advances in understanding the influence of contamination on the size of emitted drops in individual bubble bursting—either through jet drops or film drops. From a practical point of view, we aim to understand how contamination changes the size, number, or distribution of emitted drops.

A. Jet drops

We evaluate the dependence of jet drop production on contamination in the solution. Since jet drops have been widely studied, with very robust results for classic Newtonian fluids, the direct influence of several types of contamination have been examined: surfactants, thin oil layers, and proteins resulting in a viscoelastic fluid [23,25,26]. This section is mostly dedicated to the effect of surfactants.

Several experimental [54,77–79] and numerical [54,80,81] works have been dedicated to the effect of surfactants on jet drops. We recall here the mechanism for size selection, and the modifications introduced by surfactants. When the bubble cap ruptures, capillary waves travel down the underwater cavity and create the strong upwards jet when they reach the bottom. At low Laplace numbers ($\sim$1000), there is only one large capillary wave and the collapse of the cavity just before and after jet formation is self-similar [5], leading to a thin and fast jet. At high Laplace numbers ($\sim 10^5$), additional short capillary waves are present and disrupt the self-similar collapse early, leading to larger and slower jets. These short capillary waves are absent at low Laplace numbers because they are damped by viscosity before they reach the bottom of the cavity [9]. In both cases, the size of the first drop is largely determined by the radius of the jet that created it through the Rayleigh-Plateau instability. This effect is illustrated in Fig. 5(a) (top row). An optimal Laplace number for the thinnest and fastest jet is observed around La ≈ 1000, while jetting (and drop production) is suppressed at the lowest La number (La $\lesssim 500$).

The effect of surfactants on the formation of jet drops strongly depends on the Laplace number: The size of the first drop is increased at low Laplace number and decreased at high Laplace number. At high Laplace numbers, the presence of surfactant dampens the parasitic short capillary waves, resulting in a jet formation controlled by the main capillary wave and therefore thinner and faster jets than in the corresponding clean case [see Fig. 5(a) (right column) and Fig. 5(b) at La $\approx 10^5$]. At low Laplace numbers, the presence of surfactants reduces the maximal curvature reached during cavity collapse due to strong Marangoni flows. This results in a weaker main capillary wave and breaks the self-similarity of the clean case. The selected jet is therefore wider and slower [see Fig. 5(a) (left column) and Fig. 5(b) at La $\approx 2 \times 10^3$]. These results have been demonstrated both experimentally and numerically, and the multiple studies are qualitatively coherent with each other [54,77–81] (see Fig. 5). The transition from surfactant reducing drop size to increasing it seems to be around La $\approx 10^4$. In contrast to the size, the number of drops ejected shows important variability, trending towards a constant number of drops ejected until at high concentration drop production is suppressed entirely [77,79] or a slight decrease with surfactant concentration [Fig. 5(d)]. Note that the number of drops intrinsically has a higher variability than the first drop size, therefore requiring a large number of repetitions to estimate accurately.

While the above description is physically relatively clear, it remains challenging to utilize in practice and propose a general parametrization. The main hurdle being the identification of the right parameter to describe the effect of surfactants. Numerical studies use dimensionless numbers that are often not easily experimentally measurable, and experiments are often limited to using the bulk surfactant concentration that does not necessarily relate well with the macroscopic effects of surfactants. Eshima *et al.* [54] introduced a parameter that is both measurable experimentally and usable numerically, in the case of insoluble surfactants on the timescale of the capillary collapse. This parameter is obtained by measuring the surfactant equation of state $\gamma = \gamma(\Gamma)$ in a Langmuir trough by compressing the interface of a solution with an insoluble surfactant, defining an effective

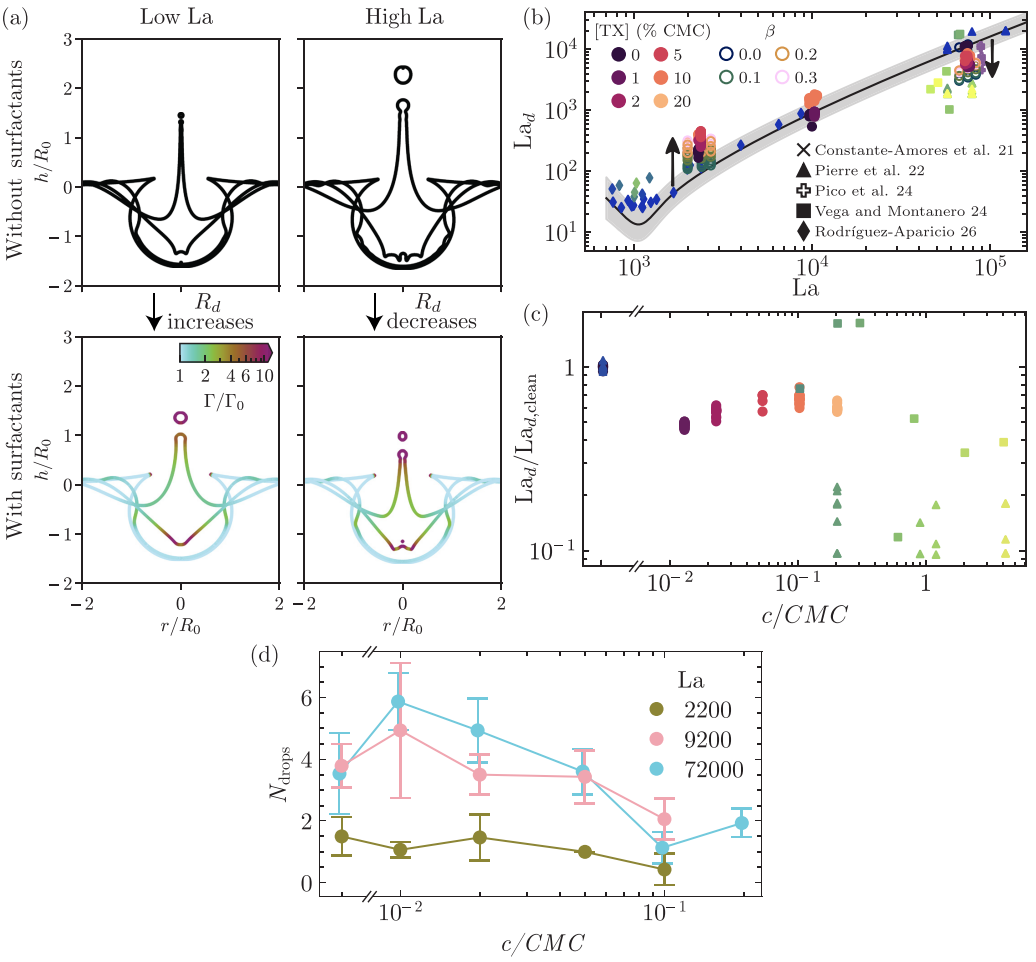


FIG. 5. Effect of surfactants on jet drop production. (a) Qualitative illustration of the effects of adding surfactants (bottom row) at low and high Laplace numbers. Color represents the dimensionless surfactant interfacial concentration (b) Drop Laplace number $La_d = r_d/\ell_\mu$ as a function of the bubble Laplace number. Closed circles correspond to experiments, with color indicating the concentration in (insoluble) surfactant Triton X-100. Open circles correspond to matching numerical simulation with color showing the dimensionless surfactant parameter β (defined in Eshima *et al.* [54]). Other markers correspond to data available in the literature. The black line and shaded area represent the average and typical spread found in the literature data (without surfactant) (c) Evolution of the drop Laplace number (normalized by the surfactant-free case) with surfactant concentration normalized by the CMC (experiments only). Markers and colors are identical to (b). Circles (from Eshima *et al.* [54]) use Triton X-100 while triangles [77] and squares [78] use SDS. Panels (a) and (b) are adapted from Eshima *et al.* [54]. (d) Evolution of the number of drops ejected at various Laplace numbers (Experimental data from Eshima *et al.* [54]) as a function of surfactant concentration. Error bars represent the standard deviation across individual measurements.

Marangoni number, and achieving quantitative agreement between laboratory experiments and numerical simulations including surfactant transport and Marangoni stresses.

Figure 5(c) illustrates the difficulties in finding a parametrization, for high Laplace numbers, plotting experimental results from Pierre *et al.* [77] (triangles) and Vega and Montanero [78] (squares), both using the surfactant SDS, and Eshima *et al.* [54] (circles) using the surfactant

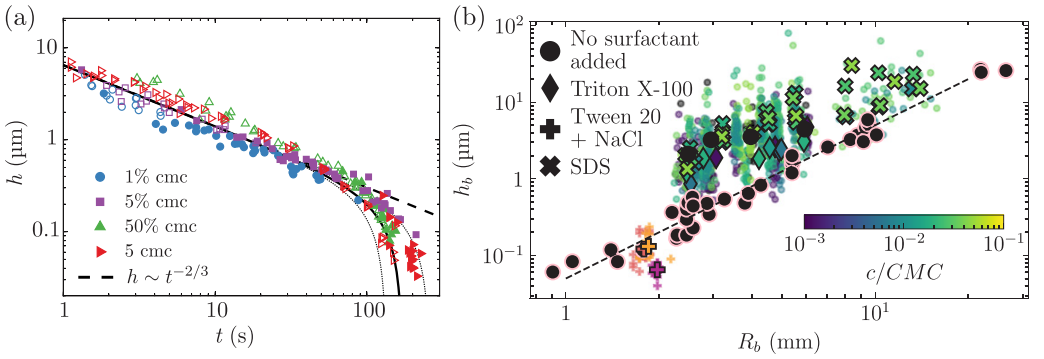


FIG. 6. Drainage of surface bubbles. (a) Drainage of a bubble cap with various concentrations of SDS (colors) in a nearly saturated atmosphere. Extracted from Poulain and Bourouiba [10]. (b) Thickness at burst h_b as a function of the bubble cap radius. Dark circles with a light edge color are extracted from Lhuissier and Villermaux [6], blue to yellow data are from Shaw and Deike [47], and orange to purple data are original. Different markers represent different surfactants, with the circles corresponding to no surfactant explicitly added. Color indicates surfactant concentration as a fraction of the CMC. Small transparent markers are individual bubble data when available and markers with a dark edge color are averages. Original set of data obtained with Tween 20 (less than 1% of the CMC) and increasing concentrations of NaCl (0, 3.5, and 35 g/l for purple, pink, and orange markers, respectively). The dashed line is a $h_b \propto R_b^2$ scaling.

Triton X-100. Even if the size reduction magnitude is consistent across studies, slightly different bubble sizes and different surfactants yield different results. In particular, it is difficult to identify at which concentration the jetting behavior transitions from clean to contaminated. The effect of some of the surfactants might be on-off instead of progressive. For practical applications it will be interesting to compare the concentrations at which significant modifications of the jetting process occur versus concentrations at which the behavior of bubbles at the surface change such as coalescence suppression or an increase in lifetime [29], as those other effects may dominate towards predicting drop production.

B. Film drainage

The direct study of the generation of film drops is difficult due to the small size of some of the drops generated, especially for the drops corresponding to submicron aerosols. Efforts in trying to understand how drop size distributions change with surfactants or salt have therefore come through the study of how surface bubble caps drain and when they burst. Indeed, as discussed in Sec. I D, in order to estimate the typical size of drops emitted from the retraction of the bubble cap (i.e., film drops) one can use the thickness of the film at burst h_b.

Surface bubble drainage has been largely studied experimentally [6,10,46,63]. Bubble caps primarily drain due to flow out towards the bulk through the foot of the bubble and due to evaporation at late times. These flows give rise to a typical thickness and timescale when evaporation becomes the main draining mechanism [59]:

$$h_\star = R_b\left(\frac{\mu D c_{\rm sat}}{\rho\gamma\ell_c}\right)^{2/5} \text{ and } t_c = R_b^2\left(\frac{\rho}{D c_{\rm sat}}\right)^{3/5}\left(\frac{\mu}{\gamma\ell_c}\right)^{2/5}, \tag{4}$$

with D and $c_{\rm sat}$, the diffusivity and saturation concentration of water vapor in air, respectively. At early times, the thickness decreases like $h \sim t^{-2/3}$, until evaporation becomes important, and the thickness decreases sharply.

Bubble drainage is largely invariant from surfactant concentration and follows the above description. See, for instance, Fig. 6(a) reproduced from Poulain and Bourouiba [10] where the drainage

curve follows a clear $h \sim t^{-2/3}$ and does not change from 1% to 5 times the CMC with SDS but also data from Shaw and Deike [47] and Pasquet *et al.* [63]. Poulain *et al.* [46] have also introduced a correction due to evaporation induced Marangoni flows. While this correction seems to be small for most sources of contamination [47], it is important when considering the effect of varying water temperature as the Marangoni and viscous effects on drainage are opposite (see Poulain *et al.* [46] and Shaw and Deike [47]). We do not consider the temperature aspect here.

The thickness at burst is harder to estimate accurately. Lhuissier and Villermaux [6] showed using a combination of their data and data from Spiel [19] that the thickness at burst, estimated using the Taylor-Culick retraction velocity, scales like $h_b \propto R_b^2$ [black markers and dashed line in Fig. 6(b)]. Experiments from Shaw and Deike [47] add to this approach with a systematic study of bursting thickness for several surfactants (blue to green markers) using the same technique. A recent study completed this data with bursting thicknesses at smaller bubble sizes and with NaCl (orange to purple markers) using thin film interferometry in the cap (similarly to Aurégan and Deike [62], Kitagawa [82], and Frostad *et al.* [83]). These experiments, while compatible with the previous data show more complexity: The bursting thickness can be much larger than suggested by the data from Lhuissier and Villermaux [6] and shows significant scatter. Of particular importance is the scaling of the bursting thickness with the bubble radius, as this relationship determines whether submicron drops can be produced by a film drop mechanism. The limited range of sizes in experiments from Shaw and Deike [47] makes it difficult to estimate the scaling, but some of the datasets (see, for instance, cases with Triton X-100 or no added surfactant) follow a scaling with an exponent less than two. However, recent experiments [with Tween 20 and NaCl, see Fig. 6(b)] show that bubbles with a cap radius less than 2 mm often reach thicknesses close to 100 nm, so that they can logically produce submicron aerosols (simply considering $r_d \approx h_b$).

Overall, one major source of uncertainty is whether the drainage relationships and the associated thickness at burst follow the same laws at smaller sizes (less than 1 mm, see Fig. 6). These bubbles are crucial for the emission of submicron film drops and produce the largest number of aerosols, but there are limited experiments that have measured the behavior of bubbles this size [20,33,84]. One alternative approach is to measure the lifetime of bubbles (how long they reside on the surface): The thickness at burst can directly be estimated if the lifetime is known using $h_b = h(\tau_i)$ with $h(t)$ the drainage curve [Fig. 6(a)] that is insensitive to contamination and τ_i the lifetime that can vary importantly with contamination and will be discussed in the next section.

C. Surface bubble lifetime

Bubble lifetime plays several roles in bubble mediated drop production: First, it can be seen as an alternative way to estimate bursting thickness. As bubbles get smaller, estimating the bursting thickness either through the film retraction velocity or through interferometry becomes particularly difficult. In contrast, bubble lifetime remains accessible for smaller bubbles. Second, bubble lifetime is required to correctly convert surface bubble measurements to a flux (see Sec. III). Predicting bubble lifetime remains, however, a challenging task, and repeatable measurements can be difficult for experimental reasons outlined in Poulain *et al.* [46]. We summarize here recent findings (using the three experimental configurations described in Sec. II) building on data on individual bubbles [59], raft and bubbling tank experiments [61], and original data.

In an extremely clean setting (devoid of any impurity in the bulk liquid besides the surfactant considered), bubble lifetime is dictated by evaporation and given by $\tau_i \propto t_c \tilde{j_e}^{-3/5}$, where $\tilde{j_e}$ is the dimensionless evaporative flux. This flux is defined as $\tilde{j_e} = \mathrm{Sh} \times (1 - \mathcal{R}_H)$, with $\mathcal{R}_H$ the relative humidity and Sh the Sherwood number, taking into account effects from natural convection and turbulent mixing in the air. This result is insensitive to surfactant concentration: See Fig. 6(a) for a very wide range of SDS concentrations (color); all data are clustered around the theoretical prediction (dashed line). In this regime, the thickness at burst is therefore close to $h_\star$. Such regime implies $h \sim R_b$ (instead of $h \sim R_b^2$ discussed above). However, when any other source of contamination is introduced (e.g., using tap water instead of deionized water or introducing salts)

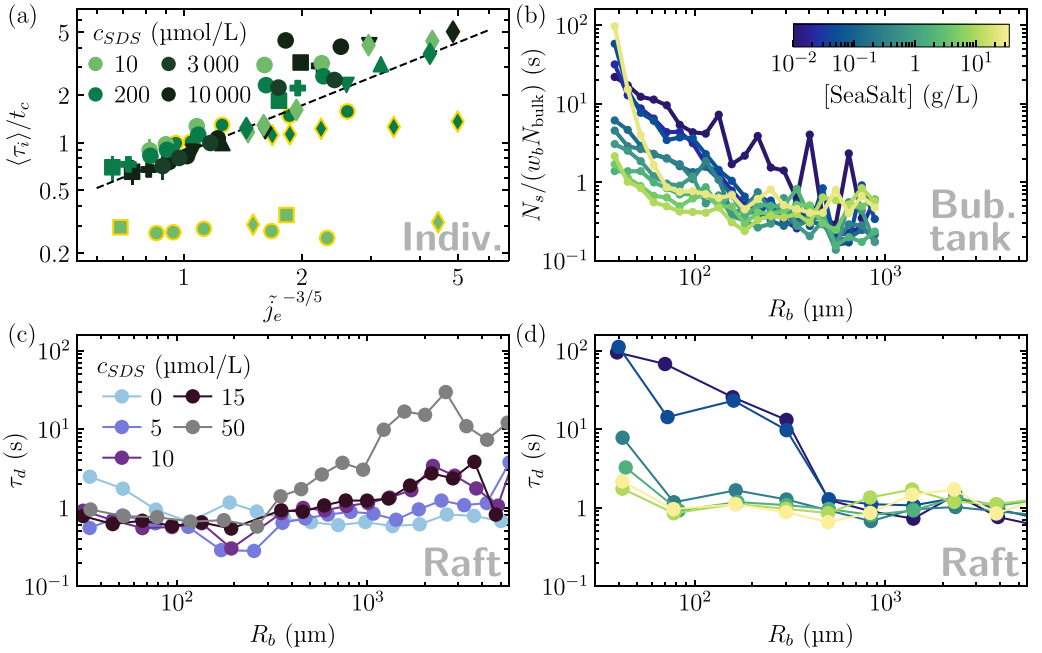


FIG. 7. Bubble lifetime measured in the different setups. (a) Evolution of the dimensionless lifetime as a function of the dimensionless evaporative rate. The timescale t_c is defined in Eq. (4) and the dashed line corresponds to the theoretical prediction when lifetime is set by the evaporation rate. Colors show different surfactant concentrations, and markers with a yellow edge color include sea salt. Markers correspond to different relative humidities (see Aurégan and Deike [59]). [(b) and (d)] Evolution of lifetime with bubble size and salt concentration (color) with two different methods. (b) Inferred lifetime τ_s using the surface to bulk conversion in the experiment Salt-1 (d) Direct measurement of the decay rate τ_d per bin size in the raft-scale experiment. (c) Evolution of lifetime τ_d with bubble size and surfactant concentration, measured through the decay rate in the raft-scale experiment.

the lifetime behavior changes: At low surfactant concentrations (less than about 100 µmol/l for SDS) the lifetime is less than t_c, meaning that bubbles burst much thicker than $h_\star$. The mean lifetime then increases with concentration until it reaches a value close to t_c at some surfactant concentration (that depends on bubble size, evaporation rate, and the type of impurity). This effect is illustrated in Fig. 7(a), where markers with a yellow edge color correspond to data obtained with sea salt at oceanic concentration, and also visible in Néel and Deike [29] with raft decay data.

Beyond the mean, the lifetime distribution is also of interest to predict drop production: Indeed, the distribution of bursting thicknesses is directly linked to the lifetime distribution, and a broad-banded distribution of lifetime can therefore result in a different mean drop size compared to a narrow-banded distribution. This distribution can have several shapes depending on the contamination of the solution [6,85,86]. In Aurégan and Deike [59], we found that the lifetime distribution is narrow-banded in either very clean (without salt) or extremely contaminated (above the CMC) solutions. In intermediate cases that are of practical use (with salt or some level of impurities) the distribution is wider, with a standard deviation comparable to the mean. Note, however, that we found that the exact shape of the distribution depends on the contamination of the solution.

Most studies on bubble lifetime have focused on bubbles with radius larger than 1 mm because of their ease of generation and observation. However, several new datasets point towards anomalous lifetime behaviors in very small bubbles. These datasets are runs Salt-1 and -2, varying salt concentration in the bubbling tank experiment with a fixed small amount of nonionic surfactant, and

a raft-scale experiment measuring decay times. In Fig. 7(b), we plot the estimated lifetime obtained by comparing the surface and bulk bubble distributions: $\tau_s(R_b) = N_s(R_b)/(N_{\text{bulk}}(R_b)w_b(R_b))$. This approach is valid as there is no coalescence thanks to the small amount of surfactant added. The lifetime obtained in this way is constant above 200 μm and increases for smaller radii, with this increase being less and less important as salinity is increased. This effect is visible for both salts (sea salt in Salt-1 and sodium acetate in Salt-2, not shown here) and is quite large as the lifetime can vary by more than an order of magnitude between low and high concentrations (note that there is no case without salt here). The absolute values of lifetime obtained are also reasonable, between 0.1 to 1 s for large bubbles and increasing to around a minute for the longest-lived bubbles. At high salt concentration, the lifetime increases again, presumably due to the presence of surfactants within the salt mixture.

Anomalous increases of bubble lifetime at small scales have been noted before [84], but, to the best of our knowledge, this decrease in lifetime with increasing salinity of the solution below a certain size has not been previously documented, most likely because of the difficulty to reliably measure the lifetime of sub-200-μm bubbles. The approach using surface and bulk bubble distributions is indirect and requires a few hypotheses (detailed in Sec. III) but allows us to probe this effect at small scales. It is striking to notice that the lifetime evolves with salinity, even when very small amounts are used (down to 10^{-2} g/l). These results are, however, consistent of the results from Aurégan and Deike [59], where we observed a strong reduction in lifetime when using salt compared to cases without any salt, although for larger bubbles.

This result obtained in the bubbling tank experiment is also consistent with measurements at the raft scale. In this original experiment, we create rafts of bubbles in a small dish with impinging jets and record the evolution of the size distribution over time (similarly to Néel and Deike [29], also used in Mazzatenta *et al.* [61]). By observing the evolution of the number of bubbles in a given size bin over time, a typical timescale $\tau_d(R_b)$ can be extracted. This timescale is shown in Figs. 7(c) and 7(d). Figure 7(c) is obtained by varying SDS concentration with an oceanic concentration of sea salt (same conditions as Surf-1), and Fig. 7(d) is obtained by varying sea salt concentration with a small amount of nonionic surfactant (same conditions as Salt-1). Strikingly, lifetime is also greatly increased by almost two orders of magnitude for low salt concentrations and for sizes below 400 μm [Fig. 7(d)]. This evolution also occurs at very low salt concentrations. We note, however, a few differences between the two experiments: The threshold below which the lifetime increases is larger in the raft-scale experiment (400 versus 200 μm) and the evolution seems more on-off than progressive like in the bubbling tank case. Overall this second experiment confirms that the small deviations visible at small sizes in the distributions in runs Salt-1 and Salt-2 are indeed due to changes in lifetime, instead of rise velocity, for instance. These experiments suggest that interesting physics is to be discovered in small, submilimetric bubbles: There is currently no evidence as to whether those bubbles follow the same drainage laws as the larger ones that have been widely studied. The very long lifetimes recorded in these new experiments are incompatible with a drainage following the laws derived in Poulain *et al.* [46], suggesting a mechanism to stabilize the bubble cap at small scales that is then disturbed in the presence of salt. Note as well that the scaling $h_b \propto R_b^2$ implies a lifetime scaling as $R_b^{1/2}$, clearly incompatible with the present data. Several studies have shown that salts can significantly slow down thin film drainage at thicknesses below 100 nm, almost halting drainage in some cases [87–91]. These results seem opposite to what is observed here; however, the effects of electrolytes on thin film stability require a careful description, for instance using the Derjaguin-Landau-Verwey-Overbeek theory to take into account the screening of electrostatic repulsion and correctly predict their effects [92].

Finally, we used the same small-scale setup to measure the decay rates of bubble in rafts, this time changing the surfactant concentration (still in the presence of 35 g/l of sea salt). Results are plotted in Fig. 7(c) where we can see yet a different type of behavior: At small scales (below 200 μm) the lifetime is essentially independent on surfactant concentration and bubble size, with a typical lifetime of the order of 1 s. For larger bubble sizes, the lifetime increases with bubble size at a

rate that increases with surfactant concentration. Fitting this part of the data we obtain a power law with R_b, with an exponent varying between 0 and 1.3. At small sizes, these data are consistent with the one varying salt concentration [Fig. 7(d)]. At large sizes we need to compare the surfactant concentrations: Figure 7(d) uses Tween 20 at 0.4% of the CMC. As a fraction of the CMC, this value corresponds to about 30 μmol/l of SDS. It is therefore interesting to note that there is no trend at large sizes in Fig. 7(d) when we could expect one using simply an the same fraction of the CMC. This effect may be due to interactions between the surfactant and salt (SDS is anionic while Tween 20 is nonionic), which can be captured as a salt concentration–dependent CMC [93–95]. We see here again the difficulty of identifying a correct parameter to compare surfactants (both solutions have surface tensions close to that of clean water).

The lifetime evolution with bubble size needs to be taken into account to correctly analyze bubble size distributions (see Secs. V A and V B), but it is for now unclear whether the lifetime variations have an effect on the typical thickness at rupture and therefore on drop production.

D. Some remarks on individual bubbles

Our understanding of surfactant effects on drop production differs vastly depending on the mode of production. On the one hand, jet drops have been widely studied, even in the presence of various types of contamination. The trends of size as a function of the Laplace number are clear, even if information on the exact number of drops emitted is currently lacking. The major remaining challenge is to identify one or several parameters describing the level of contamination and to produce a parametrization of size and number for all Laplace numbers.

On the other hand, trends regarding film drop production are much less clear, owing to the difficulty of observing submicron drops and the higher degree of stochasticity involved in film drop emission compared to jet formation. Assuming that the thickness of the film at burst is a good proxy for drop size at all levels of contamination, major challenges consist in obtaining a robust scaling for h_b with bubble size and with contamination. An additional future goal is to identify mechanisms of lifetime enhancement, in small bubbles at low salt concentrations, and in larger bubbles when contamination is important. Such lifetime information is important to estimate h_b but also to correctly use data from bubbling tanks.

V. EFFECTS OF SURFACTANTS AND SALT IN BROAD-BANDED CASES

A. Effect of surfactants on drop production

Having reviewed surfactant effects on individual bubble bursting and using the raft experiment to understand how surfactant concentration influences the size-dependent bubble lifetime, we can then study the effect of surfactant on collective bubble bursting and aerosol emission in the larger-scale bubbling tank experiment, where bubbles continuously rise, cluster at the surface, and burst in a statistically steady state. To observe the effect of surfactant on the measured bubbles and drops, we add the surfactant SDS to a base solution of artificial seawater. We consider small additions in concentration (from 5 to 50 μmol/l, with corresponding static surface tension values ranging from 71.5 to 50 mN/m). We leverage the detailed measurements of drops, bubbles, and bubble lifetime to analyze the role of surfactant in collective bursting beyond influencing bubble packing and inhibiting coalescence at the surface in Mazzatenta *et al.* [61].

We summarize here some of the findings in terms of drop production efficiency, focusing on the effect of introducing surfactant to the canonical broad-banded, oceanlike case (Surf-2 in Table I and Fig. 1). As the surfactant concentration is increased (from left to right in rows of representative images shown in Fig. 1), we observe that clusters of surface bubbles become more dense as the surfactant inhibits coalescence and leads to the formation of larger, long-lived rafts. For all of these cases, we again make detailed measurements of bubbles, drops, and particles, and we use information on the bubble lifetime from the raft experiments [Fig. 7(c)] to calculate the size

distribution of bursting bubbles [following Eq. (3)]. This result showing size-dependent lifetime in presence of surfactant must be taken into account when calculating the drop production efficiency.

To quantify the effect of surfactant on drop production, we integrate the measured bubble and drop size distributions to calculate a drop production efficiency in different bubble and drop size ranges for each contamination case. The production efficiency represents the average number of drops per bubble, found by associating a specific range of bursting bubble sizes to a corresponding range of emitted drop sizes, where the choices of bubble and drop size ranges are determined by knowledge of jet drop and submicron film drop production for individual bubble bursting. Following the canonical case (Sec. III, Fig. 3), we consider relatively large jet drops with $r_d > 10$ μm (produced by bubbles with $R_b = [130, 2500]$ μm) and submicron film drops with $r_d < 1$ μm (produced by bubbles with $R_b = [55, 1000]$ μm). For the submicron film drops, we observe an increase in the drop production efficiency of about a factor 2 as SDS concentration increases up to 10 or 15 μmol/l, where the increases in efficiency begin to level off. For the production of large jet drops, the drop production efficiency decreases significantly with increased surfactant concentration. Detailed analysis is presented in Mazzatenta *et al.* [61].

The reduction in the number of large jet drops is surprising given the data presented in Sec. IV A. Looking at Fig. 5, and assuming that contamination in the presence of sea salt has a similar effect to without it, we then expect the drop size distribution at small sizes (R_b around 50 μm, or La $\approx$ 3500, corresponding to r_d of 1 to 4 microns) to be shifted towards larger sizes and the distribution at large sizes (R_b around 1000 μm, or La $\approx$ 70 000, corresponding to r_d of 30 to 100 microns) to be shifted towards smaller sizes. For a given bubble size distribution, this combination of effects then means that the total number of drops of sizes larger than 10 μm should increase when surfactants are present, resulting in an increased efficiency. This effect is not visible here, possibly because some other process (collective effects or ionic interactions for instance) might be dominant.

In the intermediate range of 1 to 10 μm, there is no clear trend in efficiency with the concentration of surfactants, possibly because of multiple competing effects from jet and film drops that can all influence measurements within this range.

Observed increases of the number of submicron drops with surfactant concentration do not have a mechanistic interpretation for now, but the increase in lifetime with surfactant may cause bubbles to burst with a smaller film thickness, which may destabilize into numerous small drops. Future work will investigate how much these theoretical ideas are coherent with our experimental results. In addition, at these small sizes and with an important concentration of organic content in the solution, the measured submicron dry particles with the SMPS contain a significant fraction of organic material instead of being mostly salt like larger particles [96–98]. This changing composition may therefore be altering the number measured in different bins of the SMPS systems. Combined measurements of size distribution of aerosol and their composition (together with the bubble size distribution) would help understand the importance of the organic mass fraction on these questions.

B. Effect of salt on drop production

In this section, we analyze the results obtained when varying the salt concentration in the solution (datasets Salt-1 and Salt-2) in the large-scale setup. The experimental setup is detailed in Mazzatenta *et al.* [32] and Sec. II. These studies were motivated by previous experiments that have observed a peak dry aerosol size around 100 nm, regardless of the salt concentration in the bulk, even with very small values [65,99–106]. Using Eq. (2) for the conversion between drops and dry particles, the observed fixed particle size implies that one of the pathways to produce drops is sensitive to salinity, even in concentrations where salt does not affect density, viscosity, or surface tension. This discrepancy between laboratory experiments and their mechanistic explanation is, however, difficult to analyze from existing literature data: Indeed, the surface bubble size distribution directly controls the size distribution of droplets but is usually not precisely measured or reported, which prevents or complicate the interpretation of the trends seen in the measured dry particles.

We used two different salts: inorganic sea salt (dataset Salt-1), as in our other datasets, and sodium acetate (dataset Salt-2). The sodium acetate was chosen because it is a salt known to

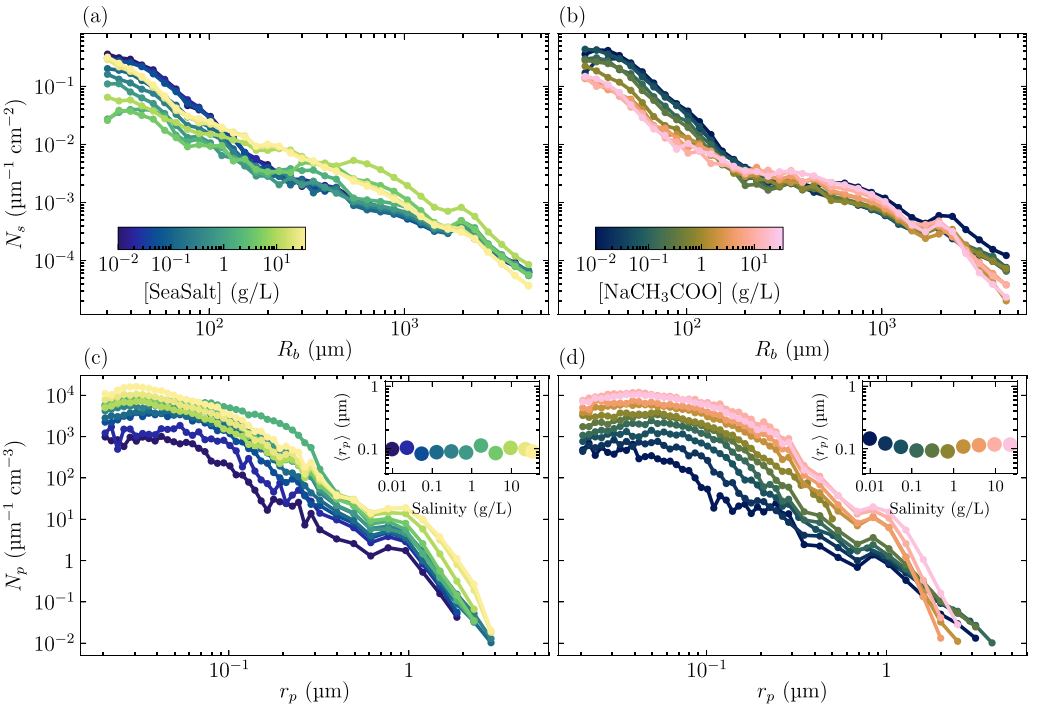


FIG. 8. Surface bubble (top) and dry aerosol (bottom) size distributions with varying concentrations of sea salt (left) and sodium acetate (right). Colors represent salt concentration. The surface bubble data corresponds to the merge of distributions from the small and wide angle views, the distributions are joined at 500 µm. The dry particle data corresponds to the merge of SMPS and OPS data, joined at 0.3 µm. Insets show the evolution of the average aerosol size with salinity.

have very little influence on bubble coalescence [88], as discussed in Dubitsky *et al.* [99], so the bubble size distribution is expected to be similar for all sodium acetate concentrations. We tested 10 salinities for each salt, ranging from 0.01 to 22 g/l in log-spaced increments, and an additional 35 g/l case was conducted for the sea salt mixture in order to mimic ocean salinity level. We also added a small amount of the nonionic surfactant Tween 20 (concentration of 0.4 µmol/l or 0.4% of the critical micelle concentration) to all solutions to inhibit bubble coalescence at all salt concentrations: This allows the bubble size distribution to remain relatively constant regardless of the salt concentration and in particular ensures the presence of small submillimetric bubbles.

We first analyze the surface bubble size distributions (Fig 8, top row): In both cases, we obtain a broad-banded size distribution of bubbles, owing to the underwater turbulence fragmenting the injected bubbles. The distributions also remain relatively similar through both ranges of salinity. In particular, we do not see the presence of a coalescence transition like in other bubbling tank studies [65], thanks to the small amount of added surfactant. There are, however, still subtle changes in the distributions: In the cases with sodium acetate [Fig. 8(b)] we can observe a monotonic decrease of the number of small bubbles below 200 µm with increasing salt concentration. We attribute this effect to differences in lifetime of the bubbles on the surface (discussed in Sec. IV C). This decrease of the number of small bubbles is also visible in the case with sea salt [Fig. 8(a)], but in addition the two cases with the highest salinity (light green and yellow) have overall more bubbles than expected. This increase is most likely due to the small amount of additional surfactants present in the sea salt preparation that we use. These results overall show that except for minute differences,

the bubble size distribution remains constant throughout all cases with different salts, as expected from the design of the experiment.

For the particles, however, we observe significant changes with salinity (Fig. 8, bottom row). The dry particle size distributions are generally also broad banded as a result of the various modes of drop production and the large size range of bubbles present in the experiment [32] and have a mean size around 100 nm (inset) consistent with previous observations [99]. For sodium acetate, we see a monotonic increase in the number of submicron particles with increased salt concentration; the value at the maximum of the distribution increases by more than an order of magnitude between the lowest and highest salinities. The peak of the distribution, however, does not appear to shift significantly from around 100 nm. This result is not consistent with Eq. (2), as if the drop size distribution was unaffected by salt, we would expect the peak size to shift to larger sizes by one order of magnitude as we vary the salt concentration by three orders of magnitude. In the case with sea salt, we also observe a general increase in the number of dry particles detected at almost all sizes; the increase in number is, however, less pronounced than in the sodium acetate case. The experiments with the highest salinities deviate from the trend, presumably due the presence of additional surfactants. In this case as well, the peak size does not appear to shift as salinity increases.

We now analyze the evolution of the aerosol production efficiency as a function of salinity. We define the efficiency as the ratio of the number concentration of aerosols to the number concentration of bubbles for a given case. In contrast to the analysis with surfactants, we do not separate the aerosols into film or jet drops and instead compute the overall number of particles and drops. The reason for this choice is that the origin of the aerosols observed is yet unclear and that usual choices of bounds correspond to aerosols generated at seawater concentration and require additional assumptions at other concentrations.

For both salts, the total number of aerosols increases with salinity by more than an order of magnitude [Fig. 9(a)]. At lower salinities, both cases are relatively well described by an increase as $n_p \sim S^{0.5}$. Both cases also seem to reach a plateau at higher salt concentration: from 1 g/l for sea salt and from 10 g/l for sodium acetate. The uncertainty on these values is low (less than 10%), except for the lowest-salinity cases where only a few salt particles are detected by the SMPS.

Separately, after accounting for the surface to bulk conversion (Sec. III) using a size and salinity dependent lifetime, the total number of bubbles remains relatively constant for all cases tested [Fig. 9(b)]. This result is in part related to the addition of a small amount of surfactants in all cases, preventing coalescence at low salinities for both salts. In the case with sea salt, we can still discern a noticeable increase in total number from a salinity of about 5 g/l, which may be attributed to a further reduction of surface bubble coalescence as this salinity corresponds to the coalescence transition for NaCl [88]. The uncertainty on this number concentration is about a factor two and mostly due the hypotheses on rise velocity and lifetime made to obtain this quantity.

Finally, we can compute the overall aerosol production efficiency as the ratio of these two quantities. As the number of aerosols n_p increases with salinity while the number of bubbles n_b is roughly constant, the number of aerosols per bubble n_p/n_b overall increases with salinity [Fig. 9(c)]. In both cases, we find an aerosol production efficiency around 30 to 50 aerosols per bubble when the salt concentration is close to seawater concentration. However, this number can both be higher and much lower at other salinities. For sodium acetate, the efficiency is increasing overall throughout the range of salinities tested, except for the most concentrated case. This increase is close to $n_p/n_b \sim S^{0.5}$ again, resulting in efficiencies as low as a few aerosols per bubble in the lowest salinities. The case with sea salt displays a similar increase at low salinities, but only up to 2 g/l. The efficiency is overall higher than in the sodium acetate case in the same range, resulting in a maximal efficiency over 100 aerosols per bubble. At higher salinities, the combination of a saturation of the number of aerosols and an increase of the number of bubbles results in a reduction of efficiency from 2 to 35 g/l. The efficiency still varies by more than an order of magnitude between the most and least efficient cases.

Overall, our results demonstrate that a full understanding requires integration of the effect of salinity in the theoretical description of sea spray emission, something currently missing. Indeed,

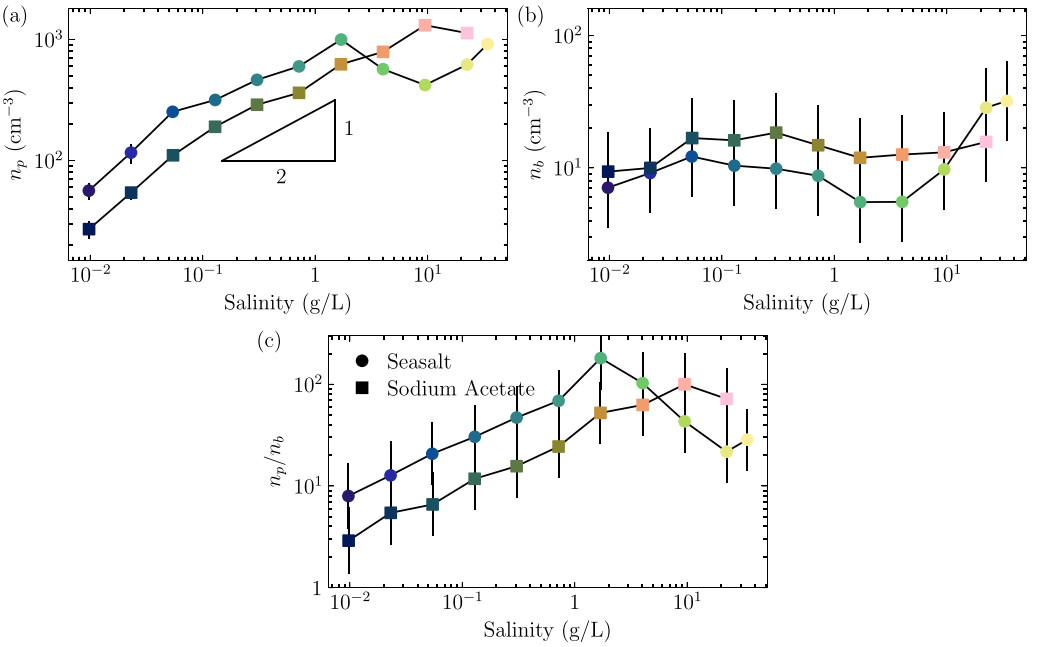


FIG. 9. (a) Evolution of the total number of dry particles n_p with salinity for both the sea salt (circles) and sodium acetate (squares). Error bars correspond to the uncertainty, estimated via bootstrapping, using the multiple scans of the OPS and SMPS for each case. (b) Evolution of the total number of bursting bubbles n_b with salinity using the same symbols. Error bars represent the uncertainty, estimated by combining errors in estimating the surface bubble distribution, the expression of the rise velocity and the lifetime. (c) Overall number of drops per bubble n_p/n_b as a function of salinity.

when the bubble size distribution is fixed, models of emission through jet or film drops predict no dependence of the size and number of the ejected drops beyond the modest effect of salts on the solution density and viscosity. In our case, the link between drops and dry aerosols would then result in a mean or peak radius of the dry aerosols varying like $S^{1/3}$ and a constant number concentration or efficiency, clearly incompatible with the present results and with other data from the literature, as noted by Dubitsky *et al.* [99]. While this sensitivity might not be critical in empirical sea spray emission function, where salinity variations are smaller, they appear as an important physics puzzle on small-scale aerosol production in salty and contaminated medium.

It could be possible that the dry particles somehow fragment before they can be measured by the SMPS or OPS: Salt crystals resulting from dried drops are not always entirely solid and can take the form of fragile hollow shells [13], and there could be a mechanism that fragments these shells into 100-nm particles when they exceed a certain size. This would both explain the fixed measured size and the increase in number as larger salinities result in more large crystals to fragment into small particles. However, we have performed additional experiments where we measure the dry particle sizes resulting from a spray of droplets of a given size (about 2 μm) with varying salinity [107]. The result do not show any indication of fragmentation occurring for the dry particles in this case.

Another effect that could partially explain our results is the size dependence of the fraction of organic materials in sea salt aerosols, this organic material being surfactants and other biological material in the bulk. Many studies have shown either in the laboratory or in the field that as aerosols get smaller, the mass fraction of organic material increases while the mass fraction of salt decreases [96–98]. This result has a small effect on the density of the particles, which then influences the measured size. More importantly, this increase in organic content means that the mass conservation

used to derive Eq. (2) is incomplete as it does not take into account organic matter. The dependence of mass fraction of organic content with size and salinity is, however, not known, and we therefore cannot currently take this effect into account. The causes for this enrichment in organic matter compared to salt are not fully understood and are usually attributed to thin film dynamics at small scales [43,66,108].

There could also be an enrichment mechanism at the bubble scale that results in all drops emitted having a similar salt concentration, irrespective of the one in the bulk. Such a mechanism may be the enrichment of the bubble cap during drainage and evaporation, similarly to what has been observed in flat films [91]. Due to the very high surface to volume ratio of thin liquid films, very high concentrations (up to the saturation) can be reached relatively quickly. With a drop production that is then independent on salinity, this hypothesis would explain the observed fixed peak size in the data. It does not, however, provide an explanation of the increasing number of aerosols with salinity.

Finally, it is possible to imagine a salinity-dependent size selection mechanism during drop production. The typical scale for ionic effects in interfacial problems is of the order of a few nanometers, and they have been shown to be able to delay underwater bubble coalescence at scales of a few tens of nanometers [87,90]. While these effects are at scales smaller than the 100-nm observed peak size, studying the contributions of ions (in combination with surfactants) to the size selection at very small scales could be an interesting avenue in the understanding of this problem.

VI. COLLECTIVE EFFECTS ON DROP PRODUCTION IN MONODISPERSE CASES

This section is dedicated to the study of the case where a narrow-banded (or monodisperse) distribution of bubbles is present at the surface and the associated changes to drop production. This configuration is unlikely in the ocean as underwater turbulence breaks up bubbles into a broad-banded size distribution. Instead, this configuration can be found in laboratory settings or in cases where bubbles are generated through liquid to air mass transfer without any agitation, such as in sparkling drinks [8,109]. In this configuration, bubbles aggregate on the surface and form rafts of a few bubbles before bursting.

We have recently shown that strong collective effects can happen in rafts of bubbles of similar millimetric sizes. Such conditions are obtained with slightly contaminated conditions where the lifetime of the bubbles is long enough to obtain rafts [29,60]. We have shown how bubbles bursting in these rafts eject jet drops much smaller than equivalent bubbles in isolation [60]. In this section, we detail this effect, and adapt Eq. (1) to account for the role of neighboring bubbles and rafts to predict the drop size distribution in run Surf-4.

In a small tank, we generated rafts of between one and a few tens of bubbles of radii around 1 mm (i.e., La $\approx 70\,000$) in solutions of deionized water, with small amounts of SDS such that surface bubble coalescence is suppressed. Note that the concentrations of SDS used here (see Fig. 10) are much smaller than the concentrations used in Sec. IV A to see a direct effect of surfactant on jet drop production ($c/\mathrm{CMC} \lesssim 0.3\%$). We use at the same time a high-speed view from the side to record the size of the jet drops and a view from the top to record the geometry of the raft and in particular the number of direct neighbors N_n of the bursting bubble. One example with $N_n = 3$ is shown in Fig. 10(a).

We found that there is a large effect of the neighboring bubbles on the properties of the ejected drops [see Fig. 10(b)]. In particular, irrespective of the bubble size and the SDS concentration within the range tested, the size of the first jet drop emitted is monotonically reduced as N_n is increased. Here the size of the first drop r_{d_1} is normalized by the size in isolation with no neighbors $r_{d_1}(N_n = 0)$, and we can see that N_n is the right parameter to describe the collective effects at the raft scale. At the same time, the velocity of the first drop and the overall number of drops ejected both increase with N_n (not shown here). We also found that this size reduction remains valid for subsequent drops beyond the first one. The size reduction is attributed to the damping of parasitic capillary waves in the collapsing cavity, due to increased dissipation from the presence of neighbors.

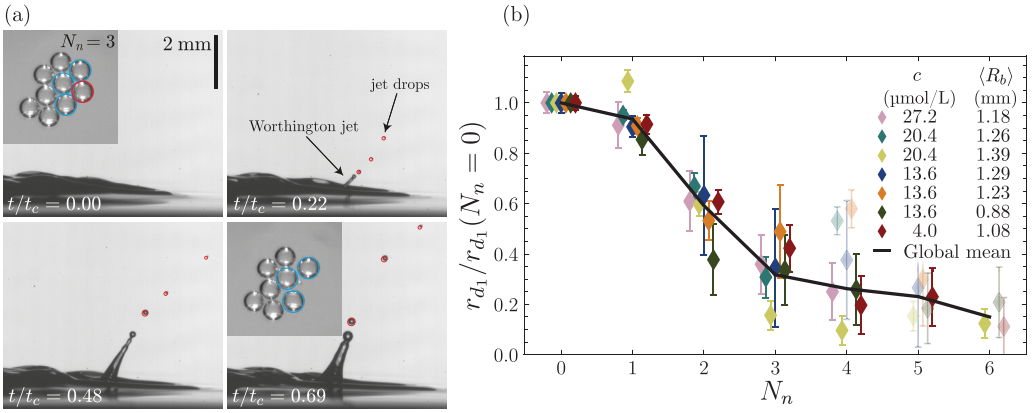


FIG. 10. Effect of neighboring bubbles on jet drop size. (a) Illustration of bubble bursting and jet formation in the presence of neighbors. The inset shows the top view of a bubble raft with the bursting bubble in red and its neighbors in blue ($N_n = 3$). The main panels show jet formation for the same bubble, with the jet tilted due to the presence of neighbors. (b) Evolution of the size of the first ejected drop r_{d_1} (normalized by the case with no neighbors) as a function of the number of neighbors. Different colors correspond to different SDS concentrations and mean bubble sizes. The black line is the average across different cases. Adapted from Aurégan *et al.* [60].

In rafts of bubbles, another phenomenon may occur where several bubbles burst in quick succession, termed multibursting. We found that when this occurs, the ejected drop sizes lose all correlation with the number of neighbors and are close to the isolated case.

With these two effects documented, we can then estimate the expected drop size distribution obtained for a whole raft of bubbles. To do so, we measure the probability that a bursting bubble has N_n neighbors for each raft size $\mathcal{R}$ in the raft experiment. The distribution for the whole raft is then constructed by fitting the drop size distribution for a given number of neighbors, taking into account all drops produced (not just the first one), and multiplying each with the corresponding probability of having N_n neighbors. The multibursting sequences are also taken into account by measuring their probability and the number of bubbles involved. The drop size distributions for a given number of neighbors can equivalently be fitted with log-normal or Gamma distributions. Note, however, that these distributions take into account that the mean size is smaller than in the isolated case and that the number of drops is increased. In addition, the drop size distribution obtained corresponds to a single bursting event (one bubble or one sequence), not to the decay of the whole raft until all bubbles have burst. Resulting drops size distributions can be found in Fig. 11(a) for increasing raft sizes $\mathcal{R}$, as a function of the dimensionless drop size $\hat{r_d} = r_d/r_d(N_n = 0)$. When rafts become larger, the mean size decreases towards smaller values, reflecting the fact that bubbles bursting with a large number of neighbors N_n become more likely (and produce smaller drops). The average number of ejected drops also increases for the same reasons. The distribution is still relatively broad due to the important probability of multibursting sequences that typically produce drop sizes around $\hat{r_d} = 1$.

We can then use this local information to estimate the drop size distribution in cases where a large number of rafts of different sizes are simultaneously present [see Fig. 11(b)]. To do so requires the knowledge of the local collective effects discussed above [i.e., the distributions for a given raft size $N_d^{\mathcal{R}}$ in Fig. 11(a)] and of the raft size distribution. We use the dataset Surf-4, originally published in Néel and Deike [29] and Néel *et al.* [31], where bubbles around 1 mm are generated, and the surfactant concentration is varied (here SDS is used). We recorded the bubble size distribution, as well as the drop sizes for relatively large drops ($r_d > 30$ μm) corresponding to jet drops only. While the bulk bubble size distribution is unchanged, since there is no salt in this case, nothing is

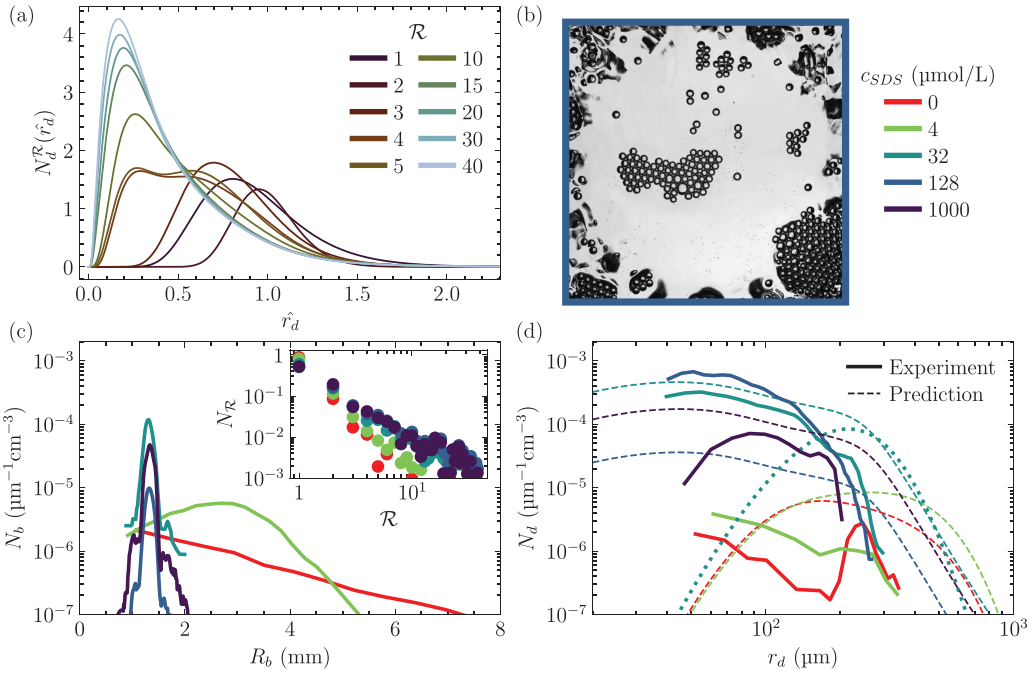


FIG. 11. Collective effects at the scale of ensembles of rafts. (a) Predicted drop size distribution for a given raft size. The drop size is normalized by the average size with no neighbors $\hat{r_d} = r_d/r_d(N_n = 0)$. Adapted from Aurégan *et al.* [60]. (b) Illustration of the typical surface bubble coverage with $c_{\mathrm{SDS}} = 128$ µmol/l. (c) Bubble size distribution (normalized with $\tau_s w_b$) for various SDS concentrations (colors). Data are from Néel *et al.* [31]. Inset: Raft size distributions for the same cases. (d) Corresponding drop size distributions: Full lines correspond to experimentally measured drops (using shadowgraphy only) and the dashed lines correspond to the prediction, using the corresponding raft size distribution and bubble size distributions.

preventing surface bubbles from coalescing at low SDS concentrations. Hence, the surface bubble size distribution is vastly different for low and high concentrations (see Fig. 11(c), distributions converted a volumetric measurement following Sec. III, with a bubble lifetime dependent only on surfactant concentration; data in Néel and Deike [29]) going from an exponentially decaying distribution to a very narrow distribution around $R_b = 1.6$ mm. In the inset is the associated raft size distribution $N_{\mathcal{R}}$, which can be seen flattening as the surfactant concentration is increased: Surface packing increases and therefore so does the likelihood of large rafts. In practice, we found that the raft size distribution can be relatively well represented using a power-law distribution with an exponent between 1.1 and 2.5, depending on surfactant concentration.

The corresponding drop size distribution can finally be estimated by using a modified version of Eq. (1) for monodisperse bubble size distributions:

$$N_d(r_d) = \frac{n_d^0(\langle R_b\rangle)}{\langle r_d^0\rangle(\langle R_b\rangle)} p^{\Sigma\mathcal{R}}(\hat{r_d}, \langle R_b\rangle) \times \int_{R_{b,\min}}^{R_{b,\max}} N_b(R_b)\mathrm{d}R_b, \tag{5}$$

where $\langle R_b\rangle$ is the mean bubble size and the superscript 0 denotes the size or number of drops associated with a case with no neighbors (i.e., identical to the introduction). $p^{\Sigma\mathcal{R}}(\hat{r_d}, \langle R_b\rangle)$ is the drop size distribution, normalized by the size and number of the isolated case. This latter distribution is computed from

$$p^{\Sigma\mathcal{R}}(\hat{r_d}, \langle R_b\rangle) = \sum_{\mathcal{R}} N_{\mathcal{R}} N_d^{\mathcal{R}}(\hat{r_d}). \tag{6}$$

Note that in contrast to the situation in the introduction, $p^{\Sigma\mathcal{R}}(\hat{r_d}, \langle R_b \rangle)$ does not integrate to 1, and its mean is not 1. This approach is only valid for nearly monodisperse distributions, like the blue cases with $c > 32$ μmol/l in Fig. 11(c).

Results from this calculation (dashed lines) are presented in Fig. 11(d) along with the corresponding experiments (full lines). Note that the span of the axes is much smaller than previous drop size distributions as we are only concerned with relatively large jet drops here. The experimental data becomes broader and shifts towards smaller drop sizes as the surfactant concentration is increased. The integration of the jet drops is performed according to Eq. (5) for the narrow-banded cases (here $c > 32$ μmol/l) and according to Eq. (1) otherwise. Indeed, collective effects are not present in broad-banded cases (see Sec. III), and how wide the bubble size distribution can be before collective effects are negligible is for now an open question.

Overall, this approach qualitatively reproduces the experimental data correctly: Collective effects broaden the drop size distribution and reduce its mean size while also correctly capturing the absolute concentration of droplets. The dotted line represents, for one of the cases, the drop size distribution without collective effects showing how small drops are completely missed. For the lower concentrations (without collective effects) the integration overestimates the width of the drop size distribution (note that the width of the drop size distribution is a free parameter in the classical integration, we use here the same values as in Mazzatenta *et al.* [32]). The integration also overestimates the number of large drops produced in all cases: This effect might be due to a direct influence of surfactants on jet drop formation as discussed in Sec. IV A, as the concentration reaches large enough values (up to 16% CMC) for this direct size reduction to become important. There are no available parametrizations of the size reduction due to surfactants on jet drop production to test this hypothesis, but the magnitude of the size reduction that would be required for the integration to agree with the data (about a factor 2) is similar to what was obtained for individual bubbles (Sec. IV A).

VII. CONCLUSION

We started this perspective from what we called the canonical oceanlike configuration: For broad-banded bubble bursting size distribution, the knowledge of the aerosol and drop size distribution can be provided by considering results obtained for individual bubble bursting.

A large number of processes that lead to drop production through bubble bursting are affected by the presence of surface-active agents in the solution. In this review, we have primarily used experiments to document several recent advances in the understanding of some of these processes: drainage, lifetime, film and jet drop ejection, coalescence, and rafts dynamics. Experimental results are discussed together with simulations and theoretical frameworks at various scales. This multitude of approaches has allowed us to explore many different processes from the scale of single bubbles or thin films to large ensembles of continuously renewed surface bubbles.

An important consideration when examining the results presented here as a whole is to understand which ones will dominate for a given surfactant concentration. Indeed, an individual bubble effect may be irrelevant for drop production if collective effects dominate at the same surfactant concentration. To compare the effects presented here we have therefore compiled several results and the ranges of concentrations over which they occur in Fig. 12, for an example surfactant (SDS), with and without the presence of sea salt. We chose SDS as it is the surfactant most commonly used in the studies above. Note that the ranges are approximates and subject to large uncertainties. Boundaries with slanted lines correspond to effects where the limit is outside of available data ranges.

This representation allows us to see that the change in jet drop size observed in Sec. IV A, essentially never occurs with bubbles in isolation: The coalescence transition, where bubble behavior changes from merging to forming rafts, occurs at concentrations much smaller than the ones where significant deviations to jet drop size have been observed. Note, though, that the exact lower bound of the modification of jet drop size is not yet clear from the data. In addition, in monodisperse rafts,

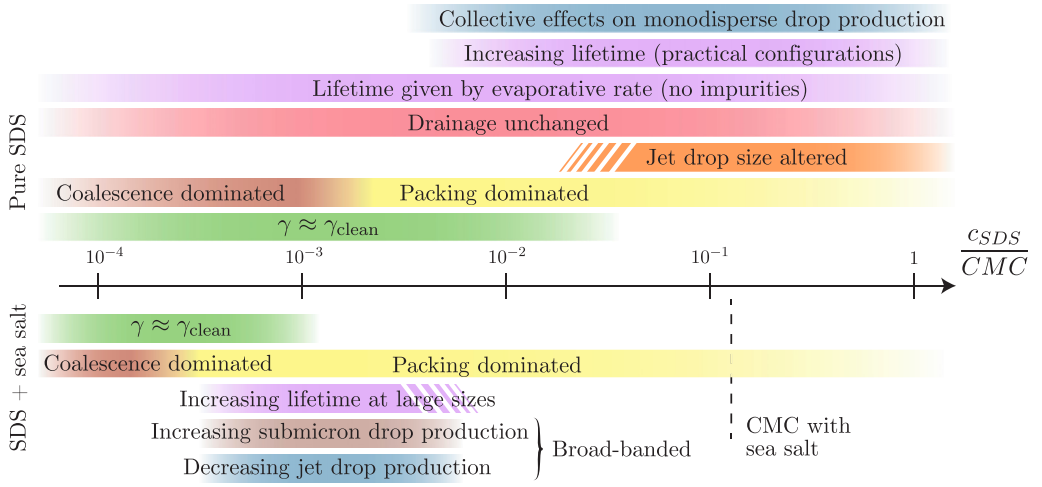


FIG. 12. Estimated thresholds of the various effects presented in this review for SDS, without any salt added (top) and with sea salt (bottom). Slanted boundaries represent limits where there is no more available data.

jet drop size is already modified by collective effects (Sec. VI) and the effects of surfactants on individual jet drop size selection should therefore be considered with neighboring bubbles.

When sea salt is present, all the relevant effects for drop production occur at concentrations about 10 times smaller than their counterpart in the case with SDS only. This is due to interaction between the surfactants (SDS is negatively charged) and the salt: As a result, the CMC is effectively reduced [94,95]. In this case, the bubbling tank experiment has allowed us to identify an increase in submicron drop production and a decrease of jet drop production at relatively low concentrations, which have not yet been linked to any specific process at the bubble scale. The effect on film drop production might be related to the film thickness at bursting (and associated lifetime), although a clear mechanistic link has not been provided. Separately, the effect of salt concentration on film drop production remains to be understood, while also affecting the transition from coalescence to packing.

Throughout this perspective, surfactant effects are represented by different physicochemical properties, including the associated surface tension gradients, their solubility, and their interaction with salts. These effects tend to be associated with different controlling parameters, or nondimensional numbers, and measurement of only the static surface tension is clearly not enough. Characterization of the equation of state $\gamma(\Gamma)$ to define a Marangoni number appears necessary, together with some characterization of solubility of the surfactant (either through a depletion length, or adsorption-desorption timescale). Questions around the renewal of the surface are also important for some processes. Finally, while the present perspective focuses on the number and sizes of the emitted aerosols in contaminated configurations, a main related challenge corresponds to associate to the chemical composition of the aerosols which be central to atmospheric or health applications.

ACKNOWLEDGMENTS

This work was supported by the National Science Foundation under Grants No. 2242512 and No. 2318816 to L.D., the Moore Foundation, the Princeton Catalysis Initiative, the National Science Foundation Graduate Research Fellowship to M.M., the High Meadows Environmental Institute Hack Award to M.M., and the High Meadows Environmental Institute CESEn Fellowship to S.M.K.. We thank Jun Eshima for discussion.

TABLE II. List of nondimensional fitting parameters used in the parametrization of drop emission.

		Equation	Value
Jet drops	Size	$\langle r_d \rangle = \chi_1 \ell_\mu (\sqrt{\mathrm{La}}(\sqrt{\mathrm{La}/\mathrm{La}_\star} - 1))^{5/4}$	$\chi_1 = 0.6$
	Number	$n_d = \chi_2 (R_b/\ell_\mu)^{-1/3}$	$\chi_2 = 30$
Film centrifuge	Size	$\langle r_d \rangle = \chi_3 R_b^{3/8} h_b^{5/8}$	$\chi_3 = 0.25$
	Number	$n_d = \chi_4 (R_b/\ell_c)^2 (R_b/h_b)^{7/8}$	$\chi_4 = 0.04$
	Film thickness	$h_b = \chi_5 R_b^2/\ell_c$	$\chi_5 = 5.43 \times 10^{-4}$
Film flap	Size	$\langle r_d \rangle = \chi_6 \ell_c (R_b/\ell_c)^{1/3}$	$\chi_6 = 1.8 \times 10^{-4}$
	Number	$n_d = 40$	

DATA AVAILABILITY

The new data that supports the findings of this article can be found in Ref. [110].

APPENDIX: NUMERICAL PREFACTORS FOR DROP PRODUCTION

Table II summarizes all prefactors used in the canonical (no surfactants) parametrization of drop production. Detailed information about the origin of each of the prefactors can be found in Deike *et al.* [15] and Mazzatenta *et al.* [32]. One exception is the fit of the size of the film flap drops, where the equation for size was missing a ℓ_c term in the above references. The prefactor χ_6 has been changed accordingly.

[1] D. C. Blanchard, The electrification of the atmosphere by particles from bubbles in the sea, Prog. Oceanogr. **1**, 73 (1963).

[2] D. C. Blanchard and A. H. Woodcock, Bubble formation and modification in the sea and its meteorological significance, Tellus A: Dyn. Meteorol. Oceanogr. **9**, 145 (1957).

[3] A. Aradian, E. Raphaël, and P.-G. D. Gennes, "Marginal pinching" in soap films, Europhys. Lett. **55**, 834 (2001).

[4] M. Bowen and B. S. Tilley, On self-similar thermal rupture of thin liquid sheets, Phys. Fluids **25**, 102105 (2013).

[5] C.-Y. Lai, J. Eggers, and L. Deike, Bubble bursting: Universal cavity and jet profiles, Phys. Rev. Lett. **121**, 144501 (2018).

[6] H. Lhuissier and E. Villermaux, Bursting bubble aerosols, J. Fluid Mech. **696**, 5 (2012).

[7] D. C. Blanchard and L. D. Syzdek, Film drop production as a function of bubble size, J. Geophys. Res.: Oceans **93**, 3649 (1988).

[8] G. Liger-Belair, G. Polidori, and P. Jeandet, Recent advances in the science of champagne bubbles, Chem. Soc. Rev. **37**, 2490 (2008).

[9] E. Ghabache, A. Antkowiak, C. Josserand, and T. Séon, On the physics of fizziness: How bubble bursting controls droplets ejection, Phys. Fluids **26**, 121701 (2014).

[10] S. Poulain and L. Bourouiba, Biosurfactants change the thinning of contaminated bubbles at bacteria-laden water interfaces, Phys. Rev. Lett. **121**, 204502 (2018).

[11] L. Bourouiba, The fluid dynamics of disease transmission, Annu. Rev. Fluid Mech. **53**, 473 (2021).

[12] F. Veron, Ocean spray, Annu. Rev. Fluid Mech. **47**, 507 (2015).

[13] R. Lewis and E. Schwartz, *Sea Salt Aerosol Production: Mechanisms, Methods, Measurements and*

Models—A Critical Review, Geophysical Monograph Series, Vol. 152 (American Geophysical Union, Washington, DC, 2004).
[14] L. Deike, Mass transfer at the ocean–atmosphere interface: The role of wave breaking, droplets, and bubbles, Annu. Rev. Fluid Mech. **54**, 191 (2022).
[15] L. Deike, B. G. Reichl, and F. Paulot, A mechanistic sea spray generation function based on the sea state and the physics of bubble bursting, AGU Adv. **3**, e2022AV000750 (2022).
[16] E. Villermaux, X. Wang, and L. Deike, Bubbles spray aerosols: Certitudes and mysteries, PNAS Nexus **1**, pgac261 (2022).
[17] J. S. Lee, B. M. Weon, S. J. Park, J. H. Je, K. Fezzaa, and W.-K. Lee, Size limits the formation of liquid jets during bubble bursting, Nat. Commun. **2**, 367 (2011).
[18] D. E. Spiel, The number and size of jet drops produced by air bubbles bursting on a fresh water surface, J. Geophys. Res.: Oceans **99**, 10289 (1994).
[19] D. E. Spiel, On the births of film drops from bubbles bursting on seawater surfaces, J. Geophys. Res.: Oceans **103**, 24907 (1998).
[20] X. Jiang, L. Rotily, E. Villermaux, and X. Wang, Submicron drops from flapping bursting bubbles, Proc. Natl. Acad. Sci. USA **119**, e2112924119 (2022).
[21] A. M. Gañán-Calvo, Revision of bubble bursting: Universal scaling laws of top jet drop size and speed, Phys. Rev. Lett. **119**, 204502 (2017).
[22] J. M. Gordillo and J. Rodríguez-Rodríguez, Capillary waves control the ejection of bubble bursting jets, J. Fluid Mech. **867**, 556 (2019).
[23] V. Sanjay, D. Lohse, and M. Jalaal, Bursting bubble in a viscoplastic medium, J. Fluid Mech. **922**, A2 (2021).
[24] B. Ji, Z. Yang, Z. Wang, R. H. Ewoldt, and J. Feng, Secondary bubble entrainment via primary bubble bursting at a viscoelastic surface, Phys. Rev. Lett. **131**, 104002 (2023).
[25] Z. Yang, Y. Liu, and J. Feng, Jet size prediction in compound multiphase bubble bursting, Phys. Rev. Lett. **134**, 214001 (2025).
[26] Z. Yang, B. Ji, J. T. Ault, and J. Feng, Enhanced singular jet formation in oil-coated bubble bursting, Nat. Phys. **19**, 884 (2023).
[27] S. Takagi and Y. Matsumoto, Surfactant effects on bubble motion and bubbly flows, Annu. Rev. Fluid Mech. **43**, 615 (2011).
[28] P. K. Farsoiya, S. Popinet, H. A. Stone, and L. Deike, Coupled volume of fluid and phase field method for direct numerical simulation of insoluble surfactant-laden interfacial flows and application to rising bubbles, Phys. Rev. Fluids **9**, 094004 (2024).
[29] B. Néel and L. Deike, Collective bursting of free-surface bubbles, and the role of surface contamination, J. Fluid Mech. **917**, A46 (2021).
[30] M.-L. E. Timmermans and J. R. Lister, The effect of surfactant on the stability of a liquid thread, J. Fluid Mech. **459**, 289 (2002).
[31] B. Néel, M. A. Erinin, and L. Deike, Role of contamination in optimal droplet production by collective bubble bursting, Geophys. Res. Lett. **49**, e2021GL096740 (2022).
[32] M. Mazzatenta, M. A. Erinin, B. Néel, and L. Deike, Linking emitted drops to collective bursting bubbles across a wide range of bubble size distributions, J. Fluid Mech. **1015**, A8 (2025).
[33] D. C. Blanchard, The size and height to which jet drops are ejected from bursting bubbles in seawater, J. Geophys. Res.: Oceans **94**, 10999 (1989).
[34] E. Ghabache, G. Liger-Belair, A. Antkowiak, and T. Séon, Evaporation of droplets in a champagne wine aerosol, Sci. Rep. **6**, 25148 (2016).
[35] C. F. Brasz, Minimum size for the top jet drop from a bursting bubble, Phys. Rev. Fluids **3**, 074001 (2018).
[36] L. Duchemin, S. Popinet, C. Josserand, and S. Zaleski, Jet formation in bubbles bursting at a free surface, Phys. Fluids **14**, 3000 (2002).
[37] L. Deike, E. Ghabache, G. Liger-Belair, A. K. Das, S. Zaleski, S. Popinet, and T. Séon, Dynamics of jets produced by bursting bubbles, Phys. Rev. Fluids **3**, 013603 (2018).

[38] A. Berny, L. Deike, T. Séon, and S. Popinet, Role of all jet drops in mass transfer from bursting bubbles, Phys. Rev. Fluids **5**, 033605 (2020).
[39] A. Berny, S. Popinet, T. Séon, and L. Deike, Statistics of jet drop production, Geophys. Res. Lett. **48**, e2021GL092919 (2021).
[40] B. Néel and L. Deike, Velocity and size quantification of drops in single and collective bursting bubbles experiments, Phys. Rev. Fluids **7**, 103603 (2022).
[41] P. L. L. Walls, L. Henaux, and J. C. Bird, Jet drops from bursting bubbles: How gravity and viscosity couple to inhibit droplet production, Phys. Rev. E **92**, 021002 (2015).
[42] F. J. Blanco–Rodríguez and J. M. Gordillo, On the sea spray aerosol originated from bubble bursting jets, J. Fluid Mech. **886**, R2 (2020).
[43] X. Wang, G. B. Deane, K. A. Moore, O. S. Ryder, M. D. Stokes, C. M. Beall, D. B. Collins, M. V. Santander, S. M. Burrows, C. M. Sultana, and K. A. Prather, The role of jet and film drops in controlling the mixing state of submicron sea spray aerosol particles, Proc. Natl. Acad. Sci. USA **114**, 6978 (2017).
[44] W. Chu, R. Zhang, X. Jiang, E. Villermaux, and X. Wang, Critical role of sea spray aerosol production pathways in particulate transfer across the sea-air interface, J. Geophys. Res.: Atmos. **130**, e2025JD044168 (2025).
[45] X. Wang, L. Dong, X. Jiang, L. Quan, X. Lu, and X. Wang, Role of jet drops from sub-100 μm bubbles in sea spray aerosol production, J. Geophys. Res.: Atmos. **131**, e2025JD045144 (2026).
[46] S. Poulain, E. Villermaux, and L. Bourouiba, Ageing and burst of surface bubbles, J. Fluid Mech. **851**, 636 (2018).
[47] D. B. Shaw and L. Deike, Film drop production over a wide range of liquid conditions, Phys. Rev. Fluids **9**, 033602 (2024).
[48] X. Jiang, L. Rotily, E. Villermaux, and X. Wang, Abyss aerosols: Drop production from underwater bubble collisions, Phys. Rev. Lett. **133**, 024001 (2024).
[49] H. Manikantan and T. M. Squires, Surfactant dynamics: Hidden variables controlling fluid flows, J. Fluid Mech. **892**, P1 (2020).
[50] H. A. Stone, A simple derivation of the time-dependent convective-diffusion equation for surfactant transport along a deforming interface, Phys. Fluids **2**, 111 (1990).
[51] M. A. Erinin, C. Liu, X. Liu, W. Mostert, L. Deike, and J. H. Duncan, The effects of surfactants on plunging breakers, J. Fluid Mech. **972**, R5 (2023).
[52] Y.-C. Liao, E. I. Franses, and O. A. Basaran, Deformation and breakup of a stretching liquid bridge covered with an insoluble surfactant monolayer, Phys. Fluids **18**, 022101 (2006).
[53] R. Yang, Z. Liu, P. K. Farsoiya, S. Popinet, and L. Deike, Surfactant effects on gravity-capillary waves, J. Fluid Mech. **1031**, A2 (2026).
[54] J. Eshima, T. Aurégan, P. K. Farsoiya, S. Popinet, H. A. Stone, and L. Deike, Size amplification of jet drops due to insoluble surfactants, Phys. Rev. Fluids **10**, 123604 (2025).
[55] G. G. Fuller and J. Vermant, Complex fluid-fluid interfaces: Rheology and structure, Annu. Rev. Chem. Biomol. Eng. **3**, 519 (2012).
[56] S. M. Burrows, O. Ogunro, A. A. Frossard, L. M. Russell, P. J. Rasch, and S. M. Elliott, A physically based framework for modeling the organic fractionation of sea spray aerosol from bubble film Langmuir equilibria, Atmos. Chem. Phys. **14**, 13601 (2014).
[57] Z. Wu, T. Aurégan, and L. Deike, Fast and slow surfactants in turbulence-driven bubble breakup, arXiv:2601.03157.
[58] J. Eshima, T. Aurégan, E. Villermaux, H. A. Stone, and L. Deike, Solubility enhanced surfactant-induced flow in air-liquid-air sheets, Phys. Rev. Lett. **137**, 144001 (2026).
[59] T. Aurégan and L. Deike, Surface bubble lifetime in the presence of a turbulent air flow, and the effect of surface layer renewal, J. Fluid Mech. **1024**, A53 (2025).
[60] T. Aurégan, N. Daniel, M. Mazzatenta, and L. Deike, Jet drop production from bubbles with neighbors, Phys. Rev. Fluids **11**, 043601 (2026).
[61] M. Mazzatenta, S. M. Koblensky, and L. Deike, Surfactant effect on collective bubble bursting and aerosol emission, arXiv:2604.21000.

[62] T. Aurégan and L. Deike, Drainage and lifetime of thin liquid films: The role of salinity and convective evaporation, J. Fluid Mech. **1012**, A18 (2025).
[63] M. Pasquet, F. Boulogne, J. Sant-Anna, F. Restagno, and E. Rio, The impact of physical-chemistry on film thinning in surface bubbles, Soft Matter **18**, 4536 (2022).
[64] M. A. Erinin, B. Néel, M. T. Mazzatenta, J. H. Duncan, and L. Deike, Comparison between shadow imaging and in-line holography for measuring droplet size distributions, Exp. Fluids **64**, 96 (2023).
[65] J. Zinke, E. D. Nilsson, P. Zieger, and M. E. Salter, The effect of seawater salinity and seawater temperature on sea salt aerosol production, J. Geophys. Res.: Atmos. **127**, e2021JD036005 (2022).
[66] R. E. Cochran, O. Laskina, J. V. Trueblood, A. D. Estillore, H. S. Morris, T. Jayarathne, C. M. Sultana, C. Lee, P. Lin, J. Laskin, A. Laskin, J. A. Dowling, Z. Qin, C. D. Cappa, T. H. Bertram, A. V. Tivanski, E. A. Stone, K. A. Prather, and V. H. Grassian, Molecular diversity of sea spray aerosol particles: Impact of ocean biology on particle composition and hygroscopicity, Chem **2**, 655 (2017).
[67] O. Wurl, W. Ekau, W. M. Landing, and C. J. Zappa, Sea surface microlayer in a changing ocean–A perspective, Elem. Sci. Anth. **5**, 31 (2017).
[68] M. Cunliffe, A. Engel, S. Frka, B. Gašparović, C. Guitart, J. C. Murrell, M. Salter, C. Stolle, R. Upstill-Goddard, and O. Wurl, Sea surface microlayers: A unified physicochemical and biological perspective of the air–ocean interface, Prog. Oceanogr. **109**, 104 (2013).
[69] G. Saliba, C.-L. Chen, S. Lewis, L. M. Russell, L.-H. Rivellini, A. K. Y. Lee, P. K. Quinn, T. S. Bates, N. Haëntjens, E. S. Boss, L. Karp-Boss, N. Baetge, C. A. Carlson, and M. J. Behrenfeld, Factors driving the seasonal and hourly variability of sea-spray aerosol number in the North Atlantic, Proc. Natl. Acad. Sci. USA **116**, 20309 (2019).
[70] D. T. McCoy, S. M. Burrows, R. Wood, D. P. Grosvenor, S. M. Elliott, P.-L. Ma, P. J. Rasch, and D. L. Hartmann, Natural aerosols explain seasonal and spatial patterns of Southern Ocean cloud albedo, Sci. Adv. **1**, e1500157 (2015).
[71] V. Fainerman, S. Lylyk, E. Aksenenko, J. Petkov, J. Yorke, and R. Miller, Surface tension isotherms, adsorption dynamics and dilational visco-elasticity of sodium dodecyl sulphate solutions, Colloids Surf., A **354**, 8 (2010).
[72] K. Sellegri, C. D. O'Dowd, Y. J. Yoon, S. G. Jennings, and G. de Leeuw, Surfactants and submicron sea spray generation, J. Geophys. Res.: Atmos. **111**, 2005JD006658 (2006).
[73] A. K. R. Salibindla, A. U. M. Masuk, S. Tan, and R. Ni, Lift and drag coefficients of deformable bubbles in intense turbulence determined from bubble rise velocity, J. Fluid Mech. **894**, A20 (2020).
[74] D. J. Ruth, M. Vernet, S. Perrard, and L. Deike, The effect of nonlinear drag on the rise velocity of bubbles in turbulence, J. Fluid Mech. **924**, A2 (2021).
[75] Z. Liu, P. K. Farsoiya, S. Perrard, and L. Deike, Direct numerical simulation of bubble rising in turbulence, J. Fluid Mech. **999**, A11 (2024).
[76] A. Rubio, E. J. Vega, M. G. Cabezas, J. M. Montanero, J. M. López-Herrera, and M. A. Herrada, Bubble rising in the presence of a surfactant at very low concentrations, Phys. Fluids **36**, 062112 (2024).
[77] J. Pierre, M. Poujol, and T. Séon, Influence of surfactant concentration on drop production by bubble bursting, Phys. Rev. Fluids **7**, 073602 (2022).
[78] E. Vega and J. Montanero, Influence of a surfactant on bubble bursting, Exp. Therm Fluid Sci. **151**, 111097 (2024).
[79] S. Rodríguez-Aparicio, A. Cebrián-García, E. J. Vega, J. M. Montanero, and M. G. Cabezas, Effect of surface-active contaminants on bubble bursting yielding the smallest first-emitted droplet, J. Fluid Mech. **1032**, A49 (2026).
[80] C. R. Constante-Amores, L. Kahouadji, A. Batchvarov, S. Shin, J. Chergui, D. Juric, and O. K. Matar, Dynamics of a surfactant-laden bubble bursting through an interface, J. Fluid Mech. **911**, A57 (2021).
[81] P. Pico, L. Kahouadji, S. Shin, J. Chergui, D. Juric, and O. K. Matar, Surfactant-laden bubble bursting: Dynamics of capillary waves and Worthington jet at large Bond number, Phys. Rev. Fluids **9**, 083606 (2024).
[82] K. Kitagawa, Thin-film thickness profile measurement by three-wavelength interference color analysis, Appl. Opt. **52**, 1998 (2013).

[83] J. M. Frostad, D. Tammaro, L. Santollani, S. Bochner de Araujo, and G. G. Fuller, Dynamic fluid-film interferometry as a predictor of bulk foam properties, Soft Matter **12**, 9266 (2016).
[84] M. Struthwolf and D. C. Blanchard, The residence time of air bubbles < 400 μm diameter at the surface of distilled water and seawater, Tellus B **36B**, 294 (1984).
[85] E. Lorenceau and F. Rouyer, Lifetime of a single bubble on the surface of a water and ethanol bath, Phys. Rev. Fluids **5**, 063603 (2020).
[86] J. Miguet, Y. Fang, F. Rouyer, and E. Rio, How does the presence of stevia glycosides impact surface bubbles stability? Colloids Surf. A **603**, 125093 (2020).
[87] S. I. Karakashev, P. T. Nguyen, R. Tsekov, M. A. Hampton, and A. V. Nguyen, Anomalous ion effects on rupture and lifetime of aqueous foam films formed from monovalent salt solutions up to saturation concentration, Langmuir **24**, 11587 (2008).
[88] M. Firouzi, T. Howes, and A. V. Nguyen, A quantitative review of the transition salt concentration for inhibiting bubble coalescence, Adv. Colloid Interface Sci. **222**, 305 (2015).
[89] D. Li, R. Manica, Z. Chen, S. Wang, Q. Liu, and H. Zhang, Bubble coalescence principle in saline water, Proc. Natl. Acad. Sci. USA **122**, e2417043122 (2025).
[90] B. Liu, R. Manica, Q. Liu, Z. Xu, E. Klaseboer, and Q. Yang, Nanoscale transport during liquid film thinning inhibits bubble coalescing behavior in electrolyte solutions, Phys. Rev. Lett. **131**, 104003 (2023).
[91] V. Ziapkoff, F. Boulogne, A. Salonen, and E. Rio, Stabilising evaporating soap films with salt, J. Fluid Mech. **1038**, A20 (2026).
[92] V. V. Yaminsky, S. Ohnishi, E. A. Vogler, and R. G. Horn, Stability of aqueous films between bubbles. Part 1. The effect of speed on bubble coalescence in purified water and simple electrolyte solutions, Langmuir **26**, 8061 (2010).
[93] M. J. Qazi, S. J. Schlegel, E. H. Backus, M. Bonn, D. Bonn, and N. Shahidzadeh, Dynamic surface tension of surfactants in the presence of high salt concentrations, Langmuir **36**, 7956 (2020).
[94] L. S. C. Wan and P. K. C. Poon, Effect of salts on the surface/interfacial tension and critical micelle concentration of surfactants, J. Pharm. Sci. **58**, 1562 (1969).
[95] S. Woolfrey, G. Banzon, and M. Groves, The effect of sodium chloride on the dynamic surface tension of sodium dodecyl sulfate solutions, J. Colloid Interface Sci. **112**, 583 (1986).
[96] K. A. Kimble, R. J. Leibensperger, C. Lee, C. Harb, E. A. Pogue, G. B. Deane, M. D. Stokes, and K. A. Prather, Wind-driven influence on submicron sea spray aerosol chemical mixing state, ACS EST Air **3**, 719 (2026).
[97] B. Gantt, N. Meskhidze, M. C. Facchini, M. Rinaldi, D. Ceburnis, and C. D. O'Dowd, Wind speed dependent size-resolved parameterization for the organic mass fraction of sea spray aerosol, Atmos. Chem. Phys. **11**, 8777 (2011).
[98] T. H. Bertram, R. E. Cochran, V. H. Grassian, and E. A. Stone, Sea spray aerosol chemical composition: Elemental and molecular mimics for laboratory studies of heterogeneous and multiphase reactions, Chem. Soc. Rev. **47**, 2374 (2018).
[99] L. Dubitsky, M. D. Stokes, G. B. Deane, and J. C. Bird, Effects of salinity beyond coalescence on submicron aerosol distributions, J. Geophys. Res.: Atmos. **128**, e2022JD038222 (2023).
[100] E. M. Mårtensson, E. D. Nilsson, G. de Leeuw, L. H. Cohen, and H.-C. Hansson, Laboratory simulations and parameterization of the primary marine aerosol production, J. Geophys. Res.: Atmos. **108**, 4297 (2003).
[101] C. A. Tyree, V. M. Hellion, O. A. Alexandrova, and J. O. Allen, Foam droplets generated from natural and artificial seawaters, J. Geophys. Res.: Atmos. **112**, 2006JD007729 (2007).
[102] J. Y. Park, S. Lim, and K. Park, Mixing state of submicrometer sea spray particles enriched by insoluble species in bubble-bursting experiments, J. Atmos. Ocean. Technol. **31**, 93 (2014).
[103] N. W. May, J. L. Axson, A. Watson, K. A. Pratt, and A. P. Ault, Lake spray aerosol generation: A method for producing representative particles from freshwater wave breaking, Atmos. Meas. Tech. **9**, 4311 (2016).
[104] C. Lv, N. T. Tsona, and L. Du, Sea spray aerosol formation: Results on the role of different parameters and organic concentrations from bubble bursting experiments, Chemosphere **252**, 126456 (2020).

[105] J. Zábori, M. Matisāns, R. Krejci, E. D. Nilsson, and J. Ström, Artificial primary marine aerosol production: A laboratory study with varying water temperature, salinity, and succinic acid concentration, Atmos. Chem. Phys. **12**, 10709 (2012).

[106] E. R. Kjærgaard, F. Hasager, S. S. Petters, M. Glasius, and M. Bilde, Bubble-mediated generation of airborne nanoplastic particles, Environ. Sci. Process. Impacts **26**, 1216 (2024).

[107] M. T. Mazzatenta, Collective bubble bursting and sea spray aerosol emission: Experiments linking bubbles and drops in the presence of surfactant and salt, Ph.D. thesis, Princeton University, 2026.

[108] X. Wang, C. M. Sultana, J. Trueblood, T. C. J. Hill, F. Malfatti, C. Lee, O. Laskina, K. A. Moore, C. M. Beall, C. S. McCluskey, G. C. Cornwell, Y. Zhou, J. L. Cox, M. A. Pendergraft, M. V. Santander, T. H. Bertram, C. D. Cappa, F. Azam, P. J. DeMott, V. H. Grassian, *et al.*, Microbial control of sea spray aerosol composition: A tale of two blooms, ACS Cent. Sci. **1**, 124 (2015).

[109] T. Séon and G. Liger-Belair, Effervescence in champagne and sparkling wines: From bubble bursting to droplet evaporation, Eur. Phys. J.: Spec. Top. **226**, 117 (2017).

[110] T. Aurégan, M. Mazzatenta, S. Koblensky, and L. Deike, Data for "advances in understanding the role of salt and surfactants on aerosol and drop emission by collective bubble bursting" [Dataset], Zenodo, 2026, 10.5281/zenodo.23158975.